HSE
Health & Safety Executive

Cyclic degradation of offshore piles

Prepared by
WS Atkins Consultants Ltd
for the Health and Safety Executive

OFFSHORE TECHNOLOGY REPORT

2000/013

HSE
Health & Safety Executive

Cyclic degradation of offshore piles

WS Atkins Consultants Ltd
Woodcote Grove
Ashley Road
Epsom
Surrey
KT18 5BW

HSE BOOKS

First published 2000

ISBN 0 7176 1911 7

CONTENTS

Page

LIST OF TABLES

LIST OF FIGURES

1. INTRODUCTION

This report presents the results of a pilot study carried out by WS Atkins Consultants Ltd into the effects of cyclic storm loading on the degradation in the capacity and the consequent reduction in the reliability of the foundations of offshore platforms. This work was funded by the Health and Safety Executive under contract OSD-D3448.

The work was carried out in collaboration with Professor Richard Jardine of Imperial College who is conducting an experimental investigation into the effects of loading history and ageing on the capacity of piles driven into sand, and in the development of appropriate numerical models for pile analysis.

The primary objectives of the study were:

1. To demonstrate the consequences of ignoring cyclic degradation in terms of reduced static capacity and reliability,

2. To define the scope for a realistic set of large and small scale tests in proportion to the extent of the problem,

3. To investigate the need for a further broad analytical study aiming at the characterisation of typical structural forms, soil and loading conditions, with respect to perceived risks due to cyclic loading. The full scope of this future study will be developed in the light of the present study following discussion with the HSE.

1.1 Experimental findings

The axial strength of cylindrical piles driven into sand has been found by experiment to be influenced by the effects of age and cyclic loading history. At the start of this study, the degradation in strength arising from cyclic loading, and the increase in strength arising from ageing were known, but only sparse experimental data was available. Subsequent experimental investigation has studied both these features and their interaction [1], [2], [3]. The main results of these studies are:

a) The severe cyclic loading that eventually causes cyclic failure of the pile brings about reductions in the static capacity that may take a long time to recover. The rate of increase in pile capacity after failure is much slower than that shown by piles that have not been failed. Pile failure in the context of the field studies was associated with significant movements of the pile.

b) Low level cyclic loading that leads to relatively small local pile to soil movements can enhance pile capacity by accelerating the ageing process.

c) Relatively high level cyclic loading leads to a progressive loss of pile capacity. The number of cycles required to degrade the pile capacity sufficiently to lead to cyclic pile failure decreases as the amplitude of the cyclic loading increases.

1.2 Soil capacity degradation model

The analyses described in this report consider a simplified model for the behaviour of a pile subject to cyclic loading. Piles were modelled using a number of discrete beam elements. The soil behaviour was modelled using laterally (p-y) and axially (t-z) orientated non-linear springs. The degradation model was applied locally to the axial t-z springs.

The model for axial pile strength and degradation derived by Imperial College had the following limitations:

1. Only sand was considered.

2. Only one soil profile was considered.

3. There was no explicit model for increases in pile capacity arising from ageing.

4. The interaction between cyclically induced enhanced ageing and cyclic degradation was not considered.

5. Only regular constant-amplitude cyclic loading was considered.

6. Degradation in tip capacity was assumed not to occur.

1.3 Assessment of overall structural capacity loss

The assessment of the effects of cyclic degradation on the full structural capacity was performed on an example North Sea platform. The example platform was assumed to remain elastic throughout the analysis, and the capacity degradation was assessed in terms of the loss in capacity of the foundation system.

An initial study was performed with the following mixture of conservative and non-conservative assumptions and limitations

1. The effects of ageing were ignored.

2. The effects of prior storms were ignored.

3. Waves of all amplitudes contributed to the degradation.

4. Interaction between ageing and degradation was ignored.

5. Storms were discretised into blocks of constant amplitude waves.

6. The overall structural degradation considered to be representative of the storm was assumed to occur just after half way through the storm.

The field tests showed that low amplitude cyclic loading leads to enhanced ageing obtained after the completion of this first set of analyses. In the light of these results, it was considered that the capacity degradation was being overestimated because the small amplitude waves

were contributing to the degradation in direct contradiction to the field tests which showed enhanced ageing for cyclic loading at these amplitudes.

In the light of the field study findings, a second study on the capacity degradation was performed using a simplified treatment of degradation in which a threshold was applied to the amplitude of the axial cyclic pile force. Cyclic loading above this threshold amplitude was assumed to lead to pile degradation, whereas cyclic loading below the threshold was assumed not to give any degradation. The threshold was calibrated against the field study results.

2. SCOPE OF WORK

The scope of work for this pilot study is described below

2.1 Soil model calibration

A solution method implemented in Mathcad for analysing the behaviour of single cyclically and axially loaded cylindrical piles in sand was developed. This spreadsheet was used for the dual purpose of providing a check for further programming work on RASOS software and for calibration of the model against experimental results. The calculation method used for axial pile capacity was that developed by Jardine and Chow [4].

Using the Mathcad spreadsheet the Imperial College soil degradation model was tested and the results used for calibration of the model against Imperial College's Dunkirk pile test results.

2.2 Development of storm model

On the basis of the data available for the example North Sea structure analysed in this study, a wave model for storms of two different return periods was developed for use in the calculation of the short-term degradation of a complete foundation system.

2.3 Implementation of cyclic degradation model into RASOS

The following items were implemented into the RASOS software in order to facilitate the degradation analysis of the full foundation system.

1. Automatic generation of the loading history as a wave passes through a structure,

2. A full cyclic hysteretic model for the cyclic p-y and t-z response of individual soil springs,

3. A facility for the automatic calculation of the degraded capacity of the t-z springs.

2.4 Pile loading for the “design” of a synthetic soil system

Axial pile loads under the extreme 100 year design storm conditions were calculated for the purposes of “designing” a synthetic soil profile for the sand used in the degradation analysis, as detailed in [2].

2.5 Degradation analysis of foundation system using full degradation model

The degradation in foundation capacity for storms of 100 and 1000 year return periods was analysed. This entailed discretising the wave loading for each block of equal amplitude waves in the discretised storm, tracing the history of local soil deformation and cumulatively applying the degradation model.

The degradation in foundation system capacity was calculated from push-over analyses at the middle and end of the storm history using the soil degradation models developed in [1], [2], and [3].

2.6 Degradation analysis of foundation system using simplified treatment which assumes a threshold

The analysis using the full degradation model of Section 2.5 was carried out under the assumption that cyclic loading of all amplitudes gives rise to some degree of degradation. Experiments performed subsequently to this analysis showed that there is interaction between cyclic loading and ageing. Low amplitude cycles, rather than degrading the pile strength, can accelerate the gain in pile strength seen during ageing.

In the light of these field study results which showed considerable interaction between cyclic degradation and cyclically induced enhanced ageing, a reanalysis of the pile system using a simplified treatment which attempted to capture this interaction was performed. The analysis assumed a threshold on the cyclic axial force component below which no degradation occurs. The degradation analysis was repeated for the two storm events using this simplified treatment of ageing-degradation interaction.

2.7 Reliability analysis

The degraded foundation system capacity and pile component capacity derived for 100 and 1000 year return period storms were used to estimate the conditional probability of foundation system failure and pile component failure during the course of these storms.

The annual probability of system and component failure were estimated from the conditional probability of failure for the individual storm events. This was done by obtaining an approximate function for the conditional failure probability as a function of storm return period and using this to account for the possibility of a storm of any size occurring in a year.

3. AXIAL CAPACITY DEGRADATION ANALYSIS OF A SINGLE PILE IN ISOLATION

The analysis of the cyclic loading behaviour of a single pile in isolation was performed with the objectives of:

1. Developing a prototype of the cyclic loading and degradation model to be implemented in RASOS where it is used for analysis of a complete platform.

2. Providing a tool for use in validation and calibration of the degradation model against the results of tests performed by Imperial College [1].

3. Validation and comparison of the model against the results of nonlinear geotechnic finite element analyses performed by Imperial College [1].

3.1 Analytical background

The single axial pile model was developed in the form of a Mathcad [5] spreadsheet and considers a single pile with a cyclically varying axial load applied at the pile head. The pile is discretised into N elastic axial elements of equal length connecting N+1 equidistant nodes. Attached to each node are non-linear axial t-z springs which model the relationship between the frictional shaft stress and strain. An additional spring is added to the bottom node to represent the pile tip load deflection relationship.

The soil spring behaviour was assumed to follow an elasto-plastic hysteretic characteristic which is typical for the behaviour of sands as specified in the recommendations of the API 20th Edition recommendations for offshore platforms [6]. The essential features of the pile modelling are depicted in Figure 1.

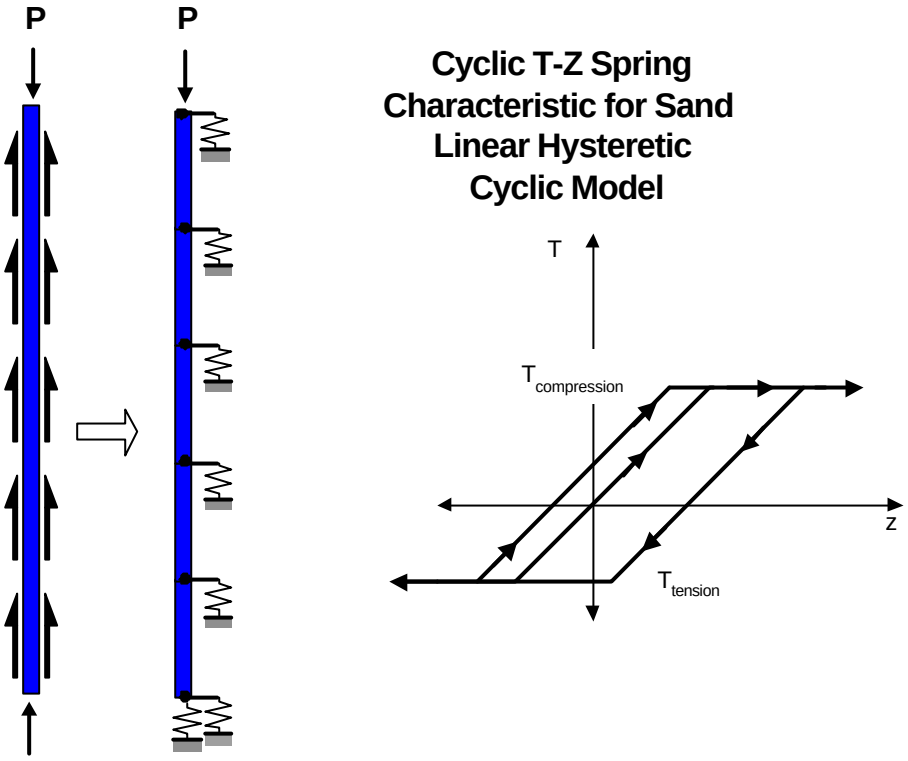

Figure 1 Pile and soil modelling

The elastic pile stiffness matrix is given by

$$\mathbf{K}_{\mathbf{Pile}} = \frac{EA}{L_{Elem}} \begin{pmatrix} 1 & -1 & & & & \\ -1 & 2 & -1 & & & \\ & -1 & \ddots & \ddots & & \\ & & \ddots & \ddots & -1 & \\ & & & -1 & 2 & -1 \\ & & & & -1 & 1 \end{pmatrix} \tag{1}$$

where E is the Young's modulus of the pile steel, A is the cross sectional pile area and L_{Elem} is the length of a single pile element.

The stiffness matrix of the soil springs is expressed in terms of an incremental secant stiffness in the form:

$$\mathbf{K}_{\mathbf{Soil}}(\Delta\mathbf{X}) = \begin{pmatrix} K_{s1}(\Delta X_1) & & & & \\ & K_{s2}(\Delta X_2) & & & \\ & & \ddots & & \\ & & & K_{sn-1}(\Delta X_{n-1}) & \\ & & & & K_{sn}(\Delta X_n) + K_{sTip}(\Delta X_n) \end{pmatrix} \tag{2}$$

where K_{si} is the secant stiffness of soil spring i, and K_{sTip} is the secant stiffness of the pile tip spring. The incremental soil secant stiffness matrix is a function of the individual soil spring displacement increment and of the current level of force in each spring.

For a given current state of pile deflections, $\mathbf{X_0}$, and internal soil spring forces, $\mathbf{F_0}$, a new loading increment, $\mathbf{DP}$, is applied at the top of the pile. The pile-soil system must satisfy the following relationship for a single loading increment

$$\left[\mathbf{K}_{\mathbf{Pile}} + \mathbf{K}_{\mathbf{Soil}}\left(\mathbf{F_0}, \Delta\mathbf{X}\right)\right]\Delta\mathbf{X} = \Delta\mathbf{P} \tag{3}$$

This solution is achieved within a load increment by iteratively deriving the displacement vector. The soil spring cyclic force-deflection relationship is then used to derive the total spring force corresponding to this deflection increment. The spring force and displacement increments are used to derive an incremental soil secant stiffness matrix from which a new displacement vector is derived. The calculations for a single iteration are given in Equations (4), (5) and (6) where i is the current iteration number.

$$\Delta\mathbf{X}_i = \left[\mathbf{K}_{\mathbf{Pile}} + \mathbf{K}_{\mathbf{Soil}\,i-1}\right]^{-1}\Delta\mathbf{P} \tag{4}$$

$$\mathbf{F}_i = \mathbf{F}\left(\mathbf{X_0}, \mathbf{F_0}, \Delta\mathbf{X}_i\right) \tag{5}$$

$$\mathbf{K}_{\mathbf{soil}_i} = \frac{\mathbf{F}_i - \mathbf{F_0}}{\Delta\mathbf{X}_i} \tag{6}$$

Iterations are repeated until convergence, measured as the difference in displacement norm between consecutive iterations, is achieved.

3.2 Definition of pile cyclic loading

Cyclic loading applied to a pile is defined in terms of the average P_{av} and cyclic P_{cy} load components which are given in terms of the maximum and minimum pile forces as:

$$P_{av} = (P_U + P_L)/2$$

$$P_{cy} = (P_U - P_L)/2$$

and are as shown in Figure 2.

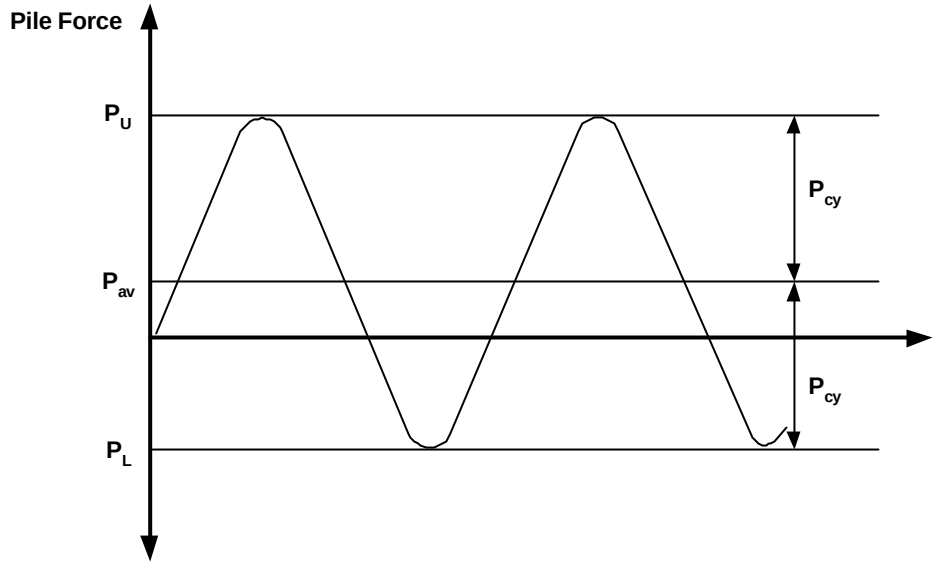

Figure 2 Definition of pile loading components

Similarly, the local shaft frictional stress is decomposed into cyclic and average components

$$\tau_{av} = (\tau_U + \tau_L)/2$$

$$\tau_{cy} = (\tau_U - \tau_L)/2$$

Although in reality the cyclic loading is of variable amplitude, this section concentrates on constant amplitude cyclic loading. This is because the majority of pile tests have been performed for constant amplitude cyclic loading conditions, and the available degradation models have also been developed and calibrated for this case.

3.3 Pile shaft shear resistance degradation

The model for shaft shear degradation developed by Imperial College from test results is described in [2].

This model assumes that pile strength degradation arises as a result of a local reduction in the radial effective stress, σ'_{r0}, of the sand. For a sequence of N cycles of constant shear stress amplitude, τ_{cy}, the reduction in radial effective stress, $\Delta\sigma'_{rcyclic}$, is given by

$$\frac{\Delta\sigma'_{rcyclic}}{\sigma'_{r0}} = A\left(\frac{\tau_{cy}}{\tau_{\max static}} + B\right)N^{C} \qquad (7)$$

where A, B and C are model parameters and $\tau_{max\ static}$ is the shaft shear capacity.

The compressive and tensile shaft friction resistance calculated using the methodology given in [4] are updated to account for this degradation according to the following equations:

$$\tau_{comp\max static} = \left(\sigma'_{r0} + \Delta\sigma'_{rcyclic} + \Delta\sigma'_{rd}\right)\tan\delta \quad (8)$$

$$\tau_{tens\max static} = 0.9\left(0.8\left(\sigma'_{r0} + \Delta\sigma'_{rcyclic}\right) + \Delta\sigma'_{rd}\right)\tan\delta \quad (9)$$

The capacities of the t-z springs are derived from the shaft shear capacity by multiplying by the surface area of pile which each spring represents. It is assumed that no degradation of the pile tip resistance occurs.

4. EXAMPLE OF DEGRADATION ANALYSIS ON A PILE

4.1 Response to cyclic loading

This section describes cyclic analyses performed with the objective of testing the Mathcad spreadsheet and gaining some understanding of pile behaviour under cyclic loading. The synthetic soil profile, developed to ensure that the piles meet the design requirements, was used for the investigation of the global structural behaviour. This profile was established by Jardine and is fully described in [2]. The pile length is 74m, divided into 25 elements. The cylindrical pile cross section is 2.134m in outer diameter and has a thickness of 70mm.

The stiffness of the t-z springs was derived by assuming that the compressive frictional resistance is fully mobilised at a deflection 2.54mm. This follows the recommended practise for platform design given in the API 20th Edition recommendations [6]. The tip spring was also assumed to have a bilinear hysteretic characteristic. The stiffness of the tip spring assumes that the tip resistance is fully mobilised at a tip displacement of one tenth of the pile diameter, again in accordance with the API 20th Edition recommendations. However, the initial tip spring stiffness was taken to be linear, whereas API 20th Edition specifies a non-linear characteristic. The difference in response is likely to be very small, particularly if the shaft friction resistance is not fully mobilised.

The distribution with depth of the local shaft frictional capacity for both overall compressive pile loading and tensile (pull-out) loading is plotted as a function of depth in Figure 3. The overall pile capacity, obtained by integrating the local shaft frictional capacity around the pile circumference and down the pile length is:

Tensile pile capacity arising from shaft frictional resistance	34 MN
Compressive pile capacity arising from shaft frictional resistance	47 MN
Compressive tip resistance	15 MN
Total compressive capacity	62 MN

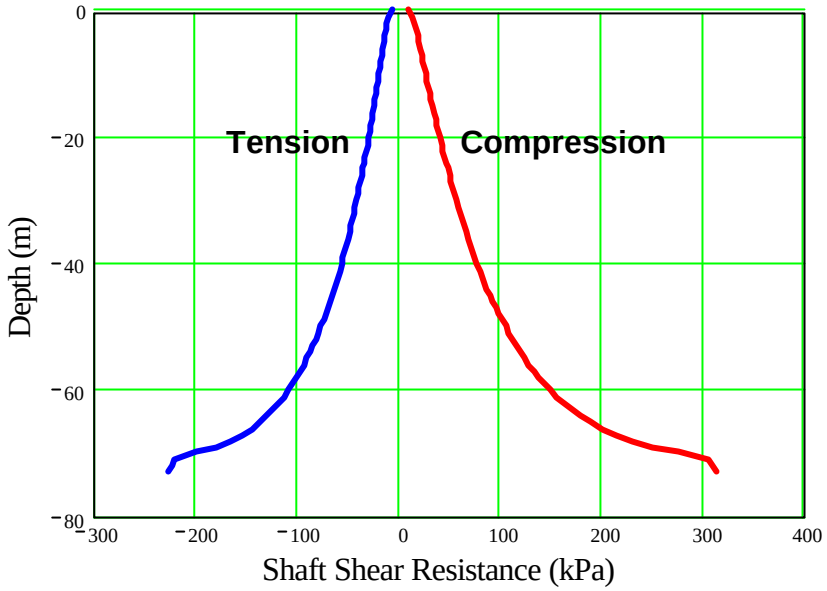

Figure 3 Synthetic pile: distribution of shaft shear resistance with depth

A cyclic loading history of five load steps was applied as follows:

P_1=10 MN
P_2=40 MN
P_3=10 MN
P_4=40 MN
P_5=10 MN

In terms of cyclic and average loading components this is:

P_{cy}=15 MN
P_{av}=25 MN

The variation in shaft shear stress following the application of the sequence of five loading steps is shown in Figure 4 whereas the vertical displacement of the pile is shown in Figure 5. It can be seen that, after the first load step, the pile response reaches a steady state response, with the cyclic and average stress components being constant.

Three zones of soil behaviour can be identified as indicated in Figure 4 by Roman numerals. Towards the top of the pile, in zone I, the soil deformation and shaft frictional stress vary in large amplitude alternating cycles, with the soil describing nominally stable hysteresis loops. Local shaft frictional capacity is fully mobilised under both senses of shearing (τ_{rz} both negative and positive). At intermediate levels, zone II, the shaft frictional capacity is fully mobilised only for pile deflections in the downwards direction and, following the initial plastic excursion at first loading, the behaviour in this region “shakes down” to a cyclic elastic behaviour. In zone III the shear resistance is not mobilised fully in either sense and the soil springs remain in their "elastic" range.

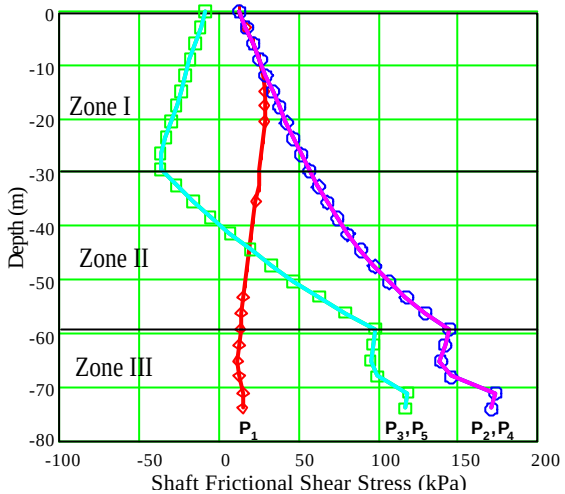

Figure 4 Synthetic pile: distribution of shaft shear stress with depth

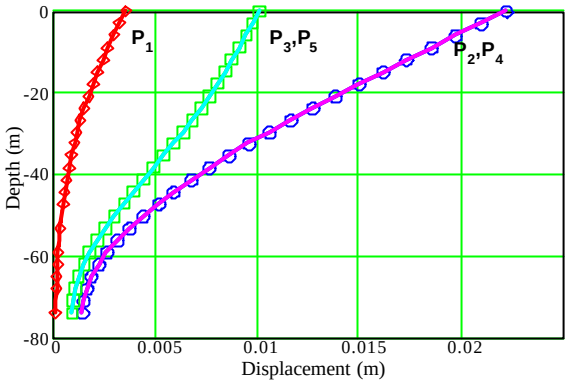

Figure 5 Synthetic pile: distribution of axial pile deflection with depth

4.2 Cyclic shaft resistance degradation

The degradation of shaft resistance was calculated in terms of the cyclic component of the shaft frictional shear stress, t_{cy}. This is plotted with depth in Figure 6 for the stable response described above.

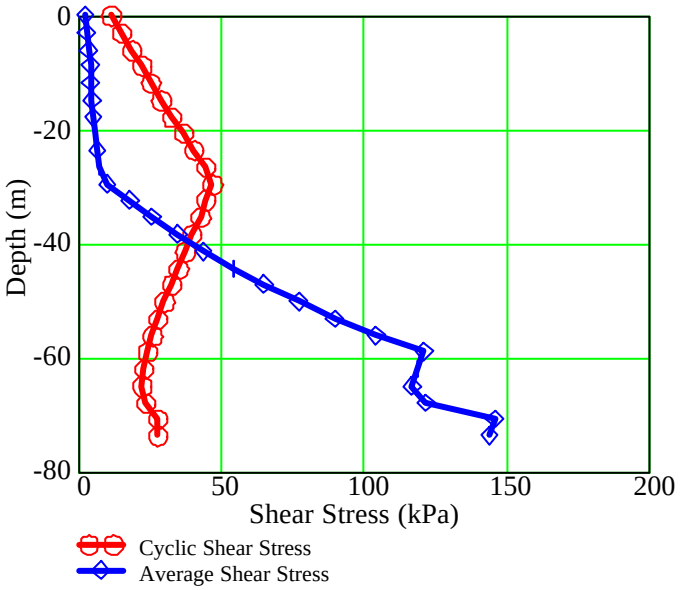

Figure 6 Synthetic pile: distribution of average and cyclic shaft shear stress with depth

An important feature of the integrated behaviour of the pile and soil is that, given a constant amplitude of force at the pile tip, the amplitude of the local stress cycles does not remain constant. For constant amplitude cyclic loading of the pile, and as a result of continual soil

capacity degradation, the zone of two-way mobilisation of shaft frictional capacity (zone I) penetrates further down the pile after each cycle of degradation with the limiting shaft shear stress envelope shrinking continuously. This growth of the fully mobilised zone down the pile and the locally increasing amplitude of stress cycles elsewhere leads to a non-uniform pattern of degradation as the cyclic loading progresses. In order to capture this effect, a single block of constant pile force cycles was divided into sub-blocks and an incremental degradation accumulation law for use between sub-blocks was applied. The degradation model for sub-blocks thus has the form:

$$r = A\left(\frac{\tau_{cy}}{\tau_{\max static}} + B\right) \tag{10}$$

$$\frac{\Delta \sigma'_{rcyclic}}{\sigma'_{r0}} = \frac{r\left(N_{tot}^{C} - \left(N_{tot} - N_s\right)^{C}\right)}{1 + r\left(N_{tot} - N_s\right)^{C}} \tag{11}$$

where

N_{tot}: Total number of cycles to date in block, including the present sub-block
N_s: Number of cycles in the present sub-block of cycles

Successive application of this updating scheme resulted in the same overall degradation in those areas that are fully mobilised in both tension and compression as the application of a single block of N_{tot} cycles given by Equation (7). When a new block of cyclic loading of a different amplitude is applied, N_{tot} is reset to zero. This simulated the observed increase in degradation rate when a new loading block was applied.

The example considered the following properties for the cyclic loading:

Number of Cycles = 200 divided into 10 sub blocks of 20 cycles

$$\frac{P_{cy}}{P_{\max comp}} = 0.32$$

$$\frac{P_{av}}{P_{\max comp}} = 0.53$$

Here $P_{\max\ comp}$ is the compressive pile capacity.

The cumulative degradation ratio of shaft frictional resistance with depth predicted by the model is shown in Figure 7. Here, the degradation factor was defined as being one minus the ratio between the degraded and original shaft strength. The increasing depth of the fully mobilised region of shear stress cycles as the loading progresses resulted in a progressive change in the shape of the degradation profile. The reduction in the degradation rate as the number of cycles increases is clearly evident from the Figure.

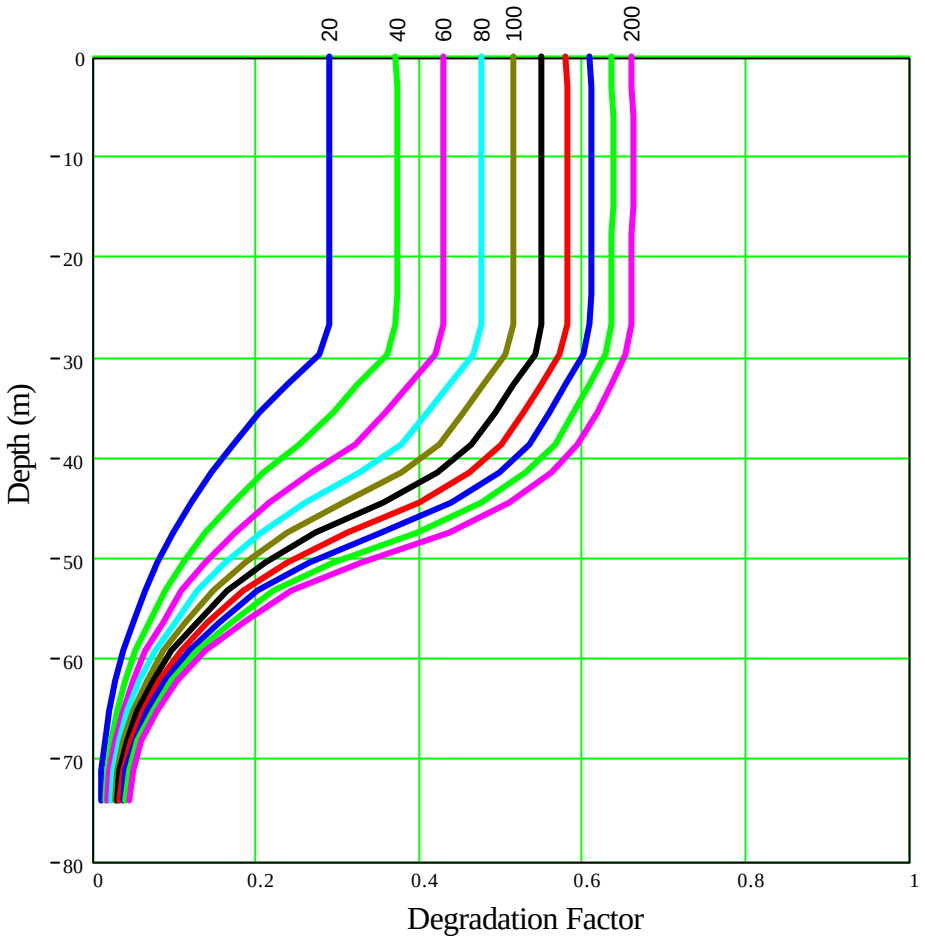

Figure 7 Progressive degradation of soil resistance with depth during the course of cyclic loading. 10 Sub-Blocks of 20 Cycles

5. CALIBRATION OF DEGRADATION MODEL

The local shaft frictional resistance degradation model was originally derived by Jardine from a series of simple shear test results on dense sands carried out on samples from a North Sea site [2]. Full scale cyclic pile tests carried out at Dunkirk by Imperial College were compared with analysis results using the Mathcad spreadsheet described above. The objective was to calibrate the pile degradation model applied to a complete pile against the test results.

Full details of this calibration exercise are reported by Jardine [1]. A brief description of the models and results is given below.

Two piles tests, denoted R3 and R4, were used for calibration of the soil degradation model. Both piles had identical material and soil properties. The piles penetrated 19.37m into the soil, had a diameter of 0.457 m and a thickness of 13.5mm. The static tensile shaft friction capacity was taken as 2.4 MN for each pile.

The pile cyclic loading was purely tensile, the applied load cycling between its maximum tensile value and zero. Pile R3 was subjected to two phases of cyclic loading. The first comprised 200 cycles between a peak tension of 1.4 MN and zero, and the second of cycles of between zero and 1.8 MN until collapse. Pile R4 was cycled between zero loading and a maximum tension of 2 MN. These cycles were applied continuously until collapse occurred.

Application of the original model derived from the cyclic shear tests was found to over-predict the number of cycles required to fail the piles in tension. On the basis of these results, it was decided to increase the factor A used in the degradation model of Equation (7) by a factor of 1.5. The final model parameters used for all the subsequent analyses were

$A = -1.245$

$B = -0.060$

$C = 0.355$

Using these revised parameters, a reanalysis of the single pile calibration tests was performed, and the results are summarised in Figure 8 to Figure 13. The results for this revised analysis over predicted the total number of cycles required to fail pile R3, giving 50 cycles in the second phase as opposed to 13 cycles required in the experiment, and under-predicted the number of cycles required to fail pile R4, 160 cycles being required to failure in the analysis as opposed to 221 in the experiment. It was concluded that these revised model parameters gave a better representation of the expected behaviour at the Dunkirk site as well as in the North Sea, in both cases the sand being less dense than that used in the original simple shear tests. The model was found to give realistic representations of the most important features of the cyclic capacity degradation seen in Dunkirk tests. One weakness was that the progressive increase in deflections observed in the experiments was not simulated by the analyses.

The results of the Dunkirk calibration analyses were also used in a comparison with the results of a series of finite element analyses performed by Imperial College. The comparison between these results is given by Jardine [1], in which it is concluded that the two analyses gave comparable initial shaft shear stress distributions, with both analyses predicting a two way cyclic loading zone developing over the top 40% of the pile shaft.

It is stated in the Introduction that reliability of a platform can suffer reduction due to short-term cyclic deterioration. To estimate the magnitude of this reduction, which is the objective of this pilot study, a number of computational steps have to be undertaken. These steps are defined in Section 2.

So far this report has addressed the first portion of these steps relating to the development and calibration of the deterministic model for the degradation analysis of a single pile. In the next part of the report, the use of this model in the context of the analysis of an overall foundation system is considered.

Pile R3: Cyclic Tension Test

Stage 1:
P_{cy} = 0.7 MN
P_{av} = -0.7 MN
N=200
5 Sub-Blocks of 40 Cycles
After 200 Cycles:

Tensile Capacity=2.15 MN
Degradation = 11.9%

Stage 2:
P_{cy} = -0.95 MN
P_{av} = -0.95 MN
Cycle until Collapse
Sub-Blocks of 10 Cycles until collapse occurs
Collapse after 50 Cycles in Stage 2

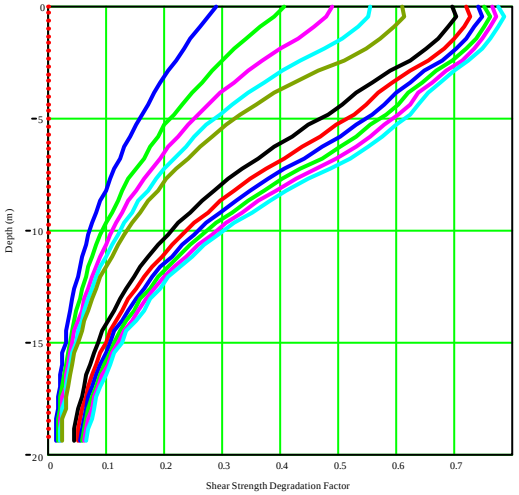

Degradation Factor Variation with Depth.
Stage 1: 5 Sub-Blocks of 40 Cycles
Stage 2: 6 Sub-Blocks 0f 10 Cycles

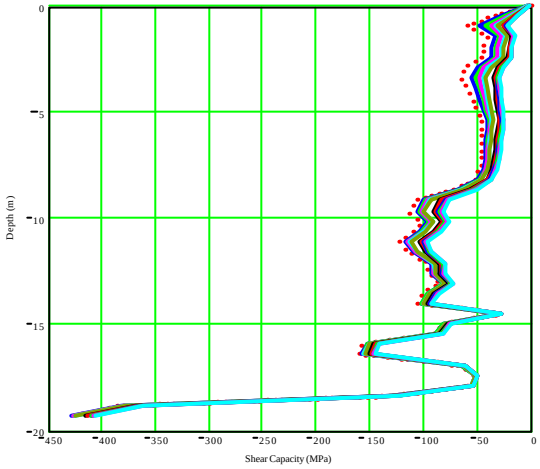

Local Shaft Frictional Resistance with Depth
Stage 1: 5 Sub-Blocks of 40 Cycles
Stage 2: 6 Sub-Blocks 0f 10 Cycles

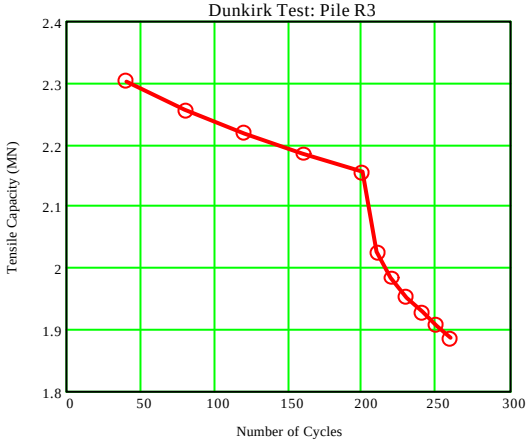

Progressive Strength Degradation

Figure 8 Summary of pile calibration analysis R3

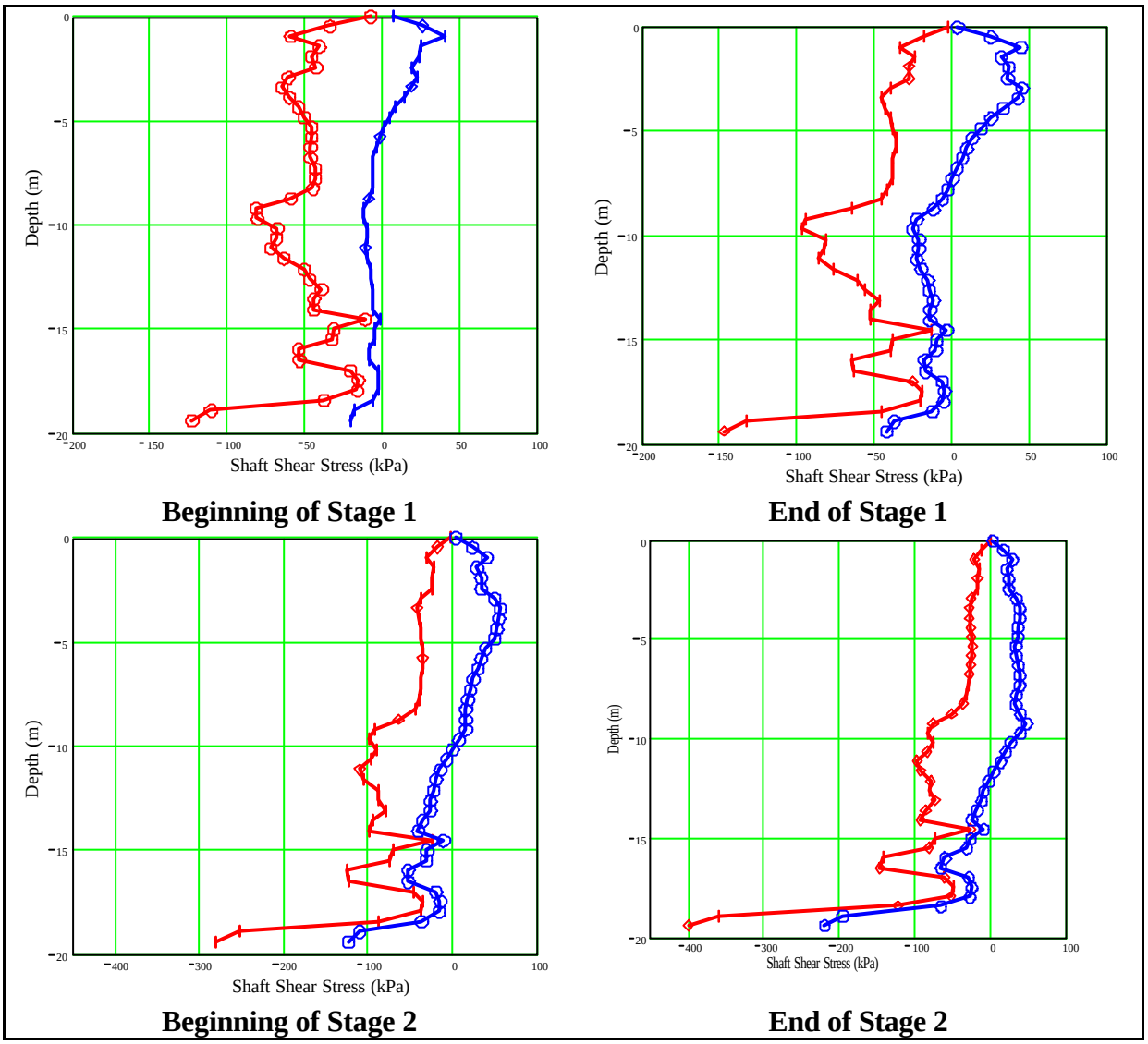

Figure 9 Summary of pile calibration analysis, R3. Shaft shear stress results

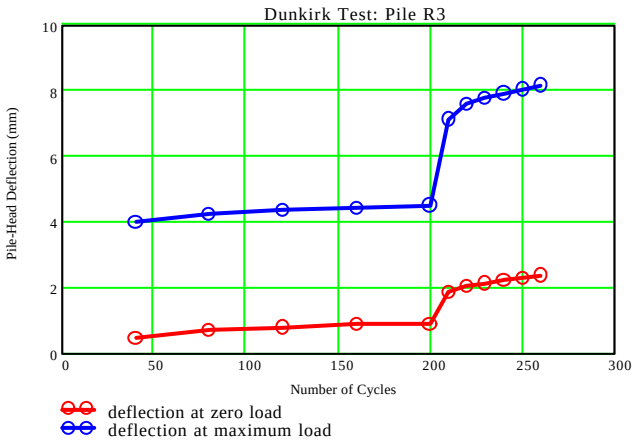

Figure 10 Calibration analysis R3: Pile head deflection

Pile R4: Cyclic Tension Test

Maximum Tension = 2.0 MN
Minimum Tension = 0.0 MN

P_{cy} = 1.0 MN
P_{av} = -1.0 MN

Cyclic Loading Model is Applied in sub-blocks of 20 cycles until collapse occurs after 160 cycles

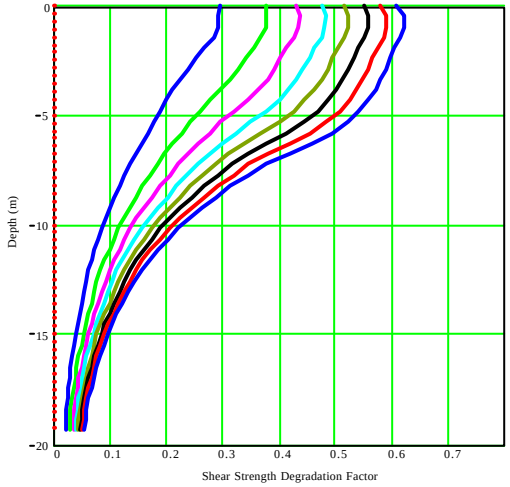

Degradation Factor Variation with Depth: 8 Sub-Blocks of 20 Cycles

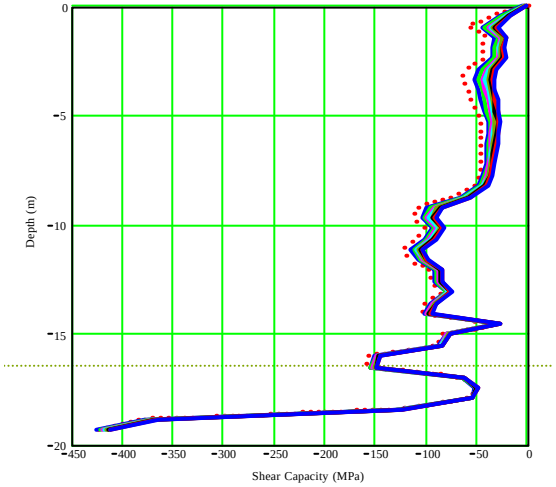

Local Shaft Frictional Resistance with Depth 8 Sub-Blocks of 20 Cycles

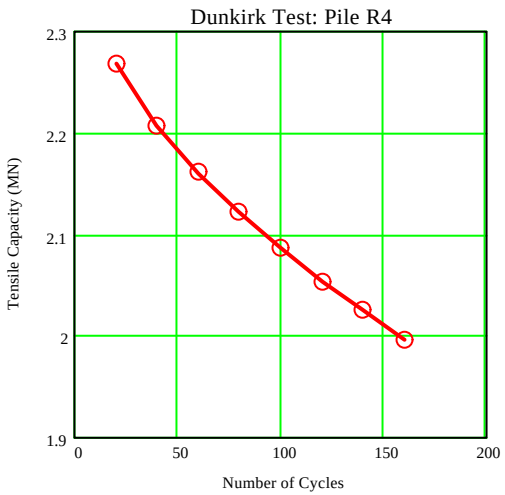

Progressive Strength Degradation

Figure 11 Summary of pile calibration analysis, R4

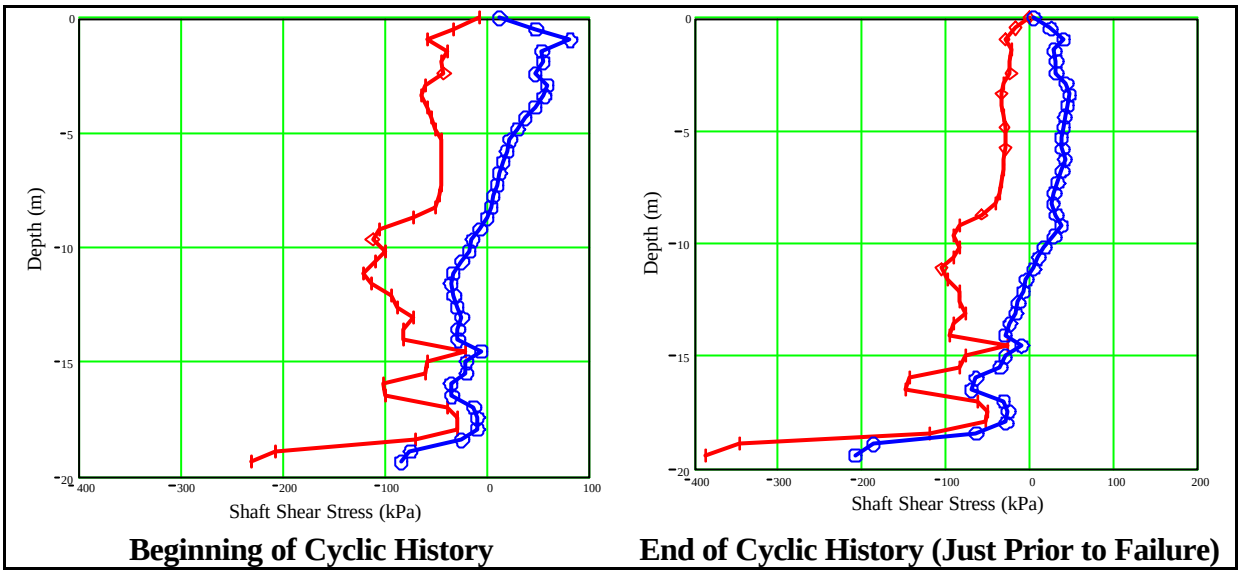

Figure 12 Summary of pile calibration analysis, R4. Shaft shear stress results

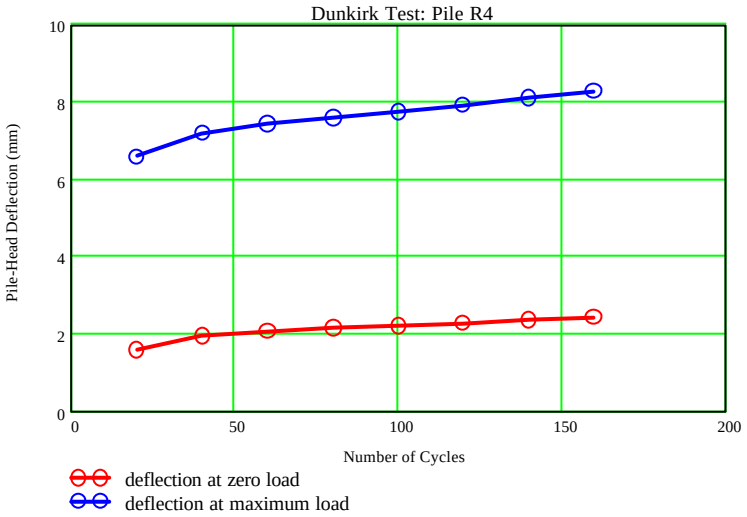

Figure 13 Calibration analysis R4: Pile head deflection results

6. CYCLIC FOUNDATION DEGRADATION STUDY FOR AN EXAMPLE NORTH SEA PLATFORM

The effects of cyclic degradation in axial pile capacity on the resistance of a complete structure were investigated using a model of an example of a central North Sea platform shown in Figure 14. The objective of using this platform is to ensure that capacity degradation is investigated in the context of realistic environmental loading and pile system effects. However, for this analysis, an artificial soil profile was used.

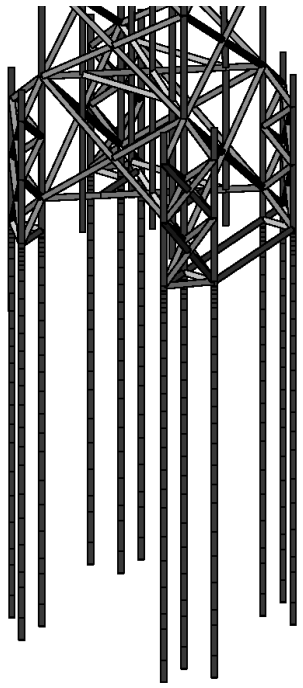

Figure 14 Model of foundation system

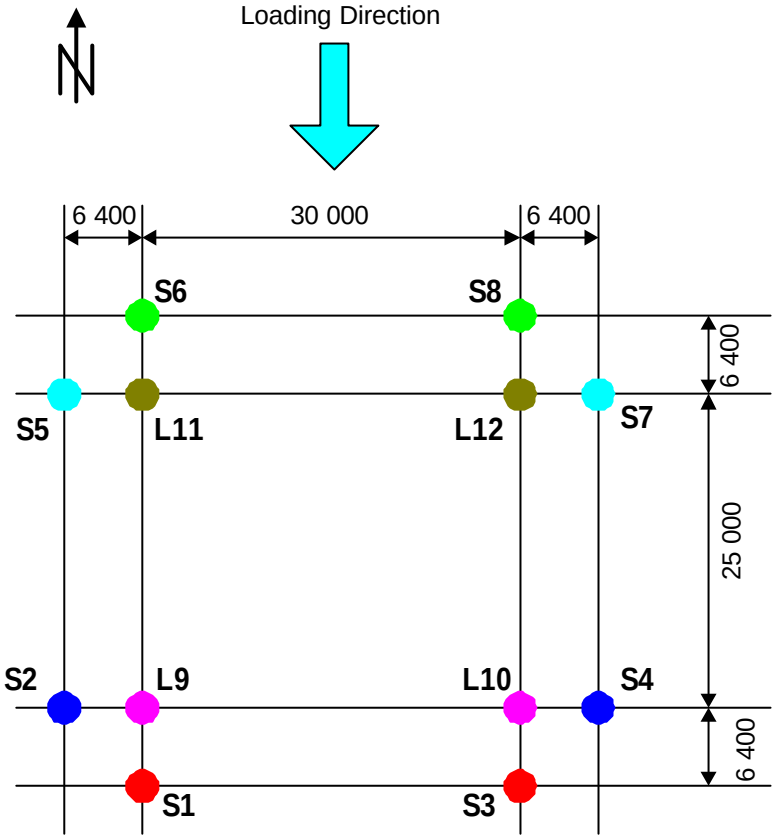

Figure 15 Pile layout

The platform has twelve piles; 4 leg piles 1.829m in diameter and 0.070m thick, and 8 skirt piles 2.134 m in diameter and 0.070 m thick, laid out in the manner illustrated in Figure 15. The pile tip is 74m below mudline level. The platform sits in 84m of water.

The structural layout accurately reflects that of a realistic North Sea platform. Similarly the environmental conditions have been chosen to accurately reflect those likely to be prevailing upon a platform in the Central North Sea.

6.1 Design environmental conditions

The design loading in the piles was obtained following the requirements of the API 20th Edition [3] recommended practice. The loading direction being considered in this study is the wave from North direction. The extreme 100 year environmental loading conditions, typical for the Central North sea are given in Table 1.

Table 1 100 year extreme environmental design conditions

Maximum Wave Height [m]	24.8
Wave Period [s]	14.0
Surface Current Velocity [m/s]	0.61
Wind Speed [m/s]	37.0
Water Depth [m]	86.2

A non-linear analysis of the pile-structure system, in which the soil is modelled using non-linear p-y and t-z springs and the structure is taken to be fully elastic, was carried out for the extreme 100 year loading plus vertical dead and live loads. The axial forces in the most loaded skirt and leg piles under this combination are tabulated in Table 2.

Table 2 Maximum pile forces under extreme environmental design conditions

	Compression	**Tension**
Skirt Piles (2134∅x70)	41.3	15.4
Leg Piles (1829∅x70)	25.1	0

The forces in the piles arising from the extreme environmental loading were multiplied by a factor of 1.5 to give the required design capacity according to the API recommendations. The critical design condition was for the skirt pile acting in compression.

On the basis of the calculated pile forces, a synthetic soil profile was evaluated by Jardine [2] using the Imperial College model for axial pile capacity in sand [4] with the objective of ensuring that the above design criteria were satisfied.

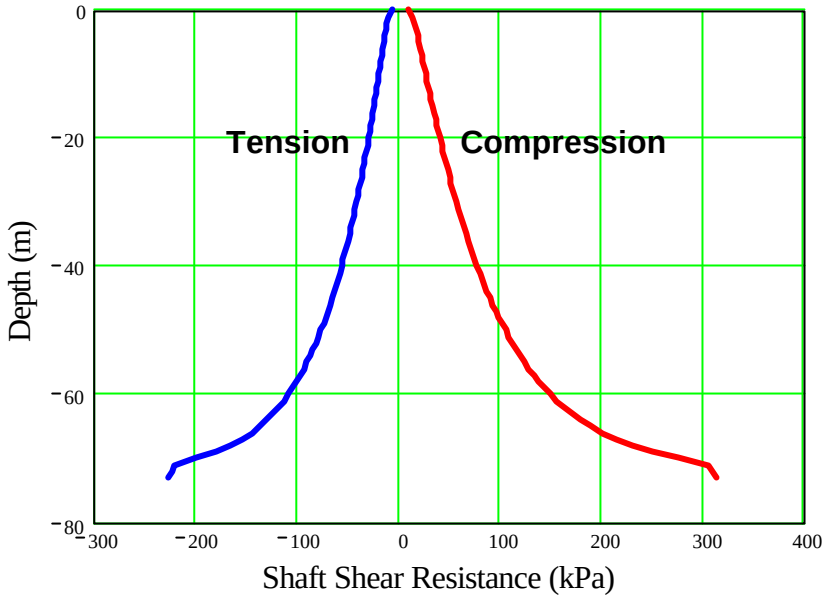

Figure 16 Synthetic soil profile: shaft shear resistance of skirt piles

The axial capacity of the two types of pile for the synthetic soil profile are given in Table 3. The distribution of shaft skin friction capacity with depth for the skirt piles is shown in Figure 16.

Table 3 Axial pile capacity

	Compressive Capacity			**Tensile Capacity**
	Shaft Capacity [MN]	Tip Capacity [MN]	Total Capacity [MN]	Total Capacity [MN]
Skirt Pile	47	15	62	34
Leg Piles	39	13	52	29

The critical soil profile has been "designed" to lead to the compressive capacity of the skirt pile being the critical design criterion. The tensile skirt pile capacity, and the leg pile capacity, not being design-critical, will have reserve capacity. This, combined with the overall foundation system redundancy, ensures that the foundation system will resist loading considerably greater than the design loading.

6.2 Pile system capacity

The capacity of the pile system was determined by performing a non-linear pushover analysis of the platform in which the dead and live loads were applied to the structure and the 100 year extreme design environmental loading was incremented until collapse of the pile system occurred. The factor on the 100 year extreme loading at the point of collapse provides the measure of Reserve Strength Ratio (RSR). Failure of structural elements was assumed not to occur, the jacket being modelled as elastic. However the non-linear p-y and t-z soil spring characteristics were used, and plastic behaviour of the pile steel was modelled. The capacity calculation was carried out for unaged piles that are nominally 50 days old.

The relationship between the environmental load factor and the lateral deflection at the top of the platform and at the pile head is shown in Figure 17. The final collapse mode of the platform is shown, to an exaggerated scale, in Figure 18. Figure 19 shows the individual pile axial force vs. axial deflection relationship. The RSR of the undegraded pile system can be seen to be 2.95.

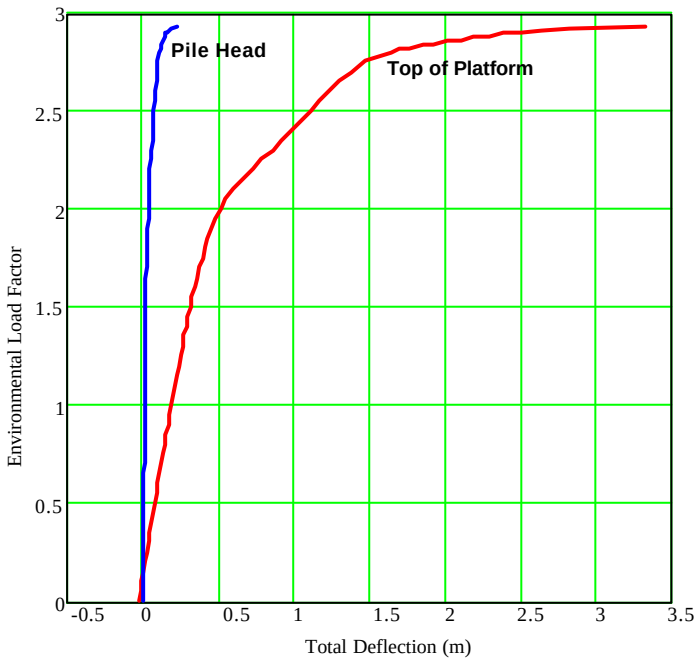

Figure 17 Undegraded pile system: environmental load vs. lateral deflection

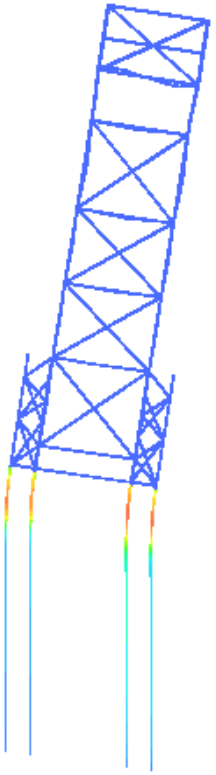

Figure 18 Pile system collapse mode

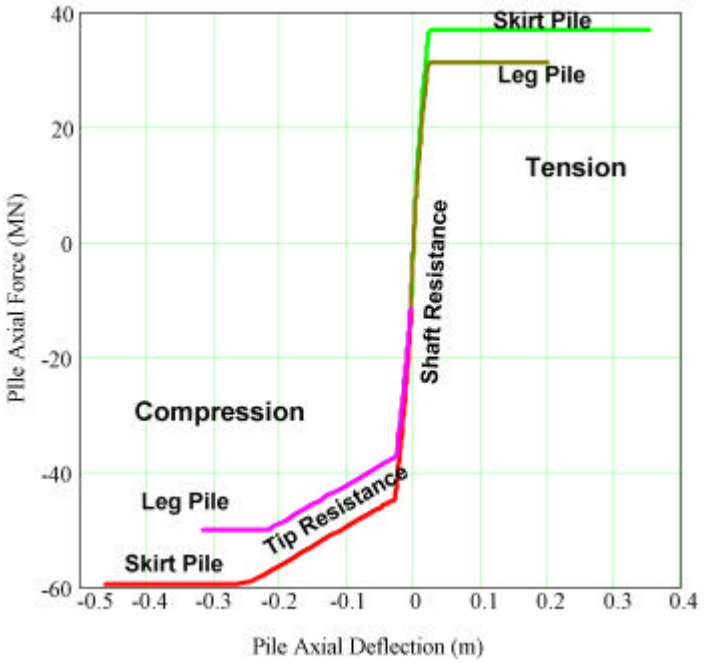

Figure 19 Individual pile axial load-deflection characteristic

The axial pile behaviour, shown in Figure 19, was characterised by four distinct modes. The stiffest part of the behaviour occurred in the region where the shaft friction resistance was being mobilised. This behaviour was the integrated effect of the mobilisation of shaft resistance down the pile. Once the shaft resistance had been fully mobilised in compression, additional resistance to axial loading was offered by the pile tip. This portion of the axial load-deflection behaviour was considerably less stiff than before the shaft resistance had been fully mobilised. Once the tensile or compressive capacity was fully mobilised, axial deflections could increase with no change in axial loading.

Figure 20 shows the relationship between the axial forces in the piles and the environmental load factor. Figure 21 shows the axial pile-head deflections. At zero environmental load, the axial loading in the piles arose from the dead and live vertical loading. There was some eccentricity in this loading which can be seen from the higher compressive axial forces in the eastern-most piles compared to the western piles. The environmental loading resulted in lateral and overturning forces on the foundation system. The overturning was resisted by increased compressive loading in the eight southern-most piles and increased tensile forces in the eight northern-most piles. At an environmental load factor of about 1.4, the shaft resistance in the outer-most compressive skirt pile, S3 was fully mobilised. At this point the axial stiffness of pile S3 was significantly reduced. The additional loading, which would otherwise be taken by pile S3, was redistributed amongst the other piles which showed a relative increase in loading, most notable in piles S4 and L10. Pile S3 showed a significant decrease in the rate at which its axial load increased. Similar behaviour was seen for pile S4 whose shaft resistance was fully mobilised at an environmental load factor of 1.6.

The first pile to actually reach its full capacity was the outermost tensile skirt pile, S6 at an environmental load factor of 1.9, closely followed by the failure of its companion pile S8 at a

load factor of 2.05. At this point all the compressive piles had fully mobilised shaft resistance. The resulting increase in over-turning angle and reduction in over-turning stiffness can be clearly seen from the environmental load factor vs. top of platform displacement plot of Figure 17 and the individual axial pile displacement plot of Figure 21.

Final collapse of the foundation system was reached once the axial capacity of the inner compressive skirt piles S2 was reached. At this point the platform was free to rotate around piles S7, L11, L12 and S5. However a small amount of further capacity was available from the rotational capacity of the piles. The final failure mode, shown in Figure 18, comprised an overall overturning mode of the platform which required for kinematic consistency, full mobilisation of the axial deformation of the piles and the rotation capacity of the pile heads. The pile head rotation arose as a result of the combined effects of plastic hinge formation at some distance down the pile, and the lateral failure of the soil above this hinge.

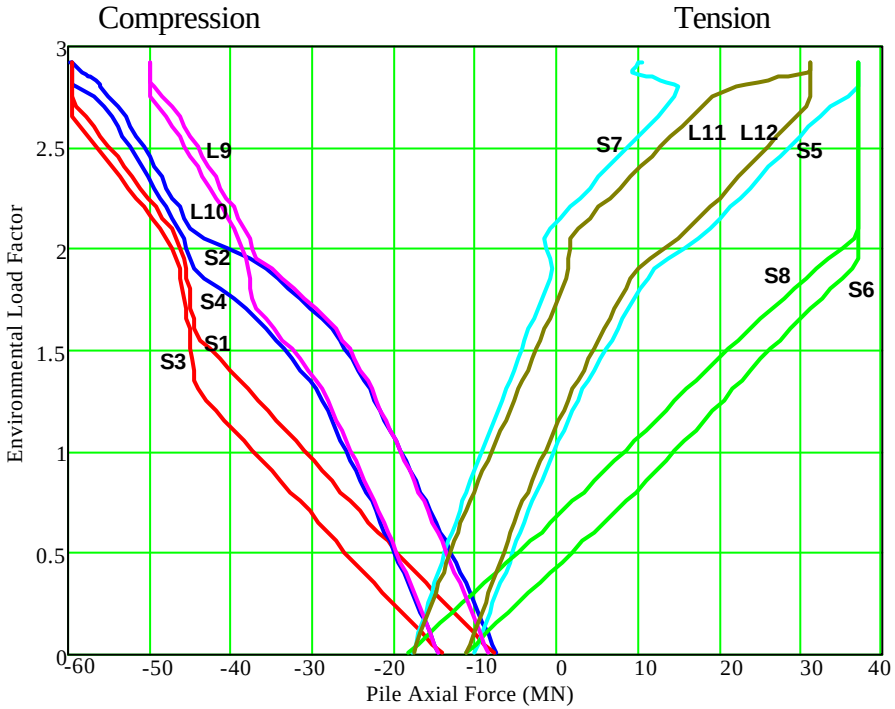

Figure 20 **Undegraded foundation system: axial pile load vs. environmental load factor**

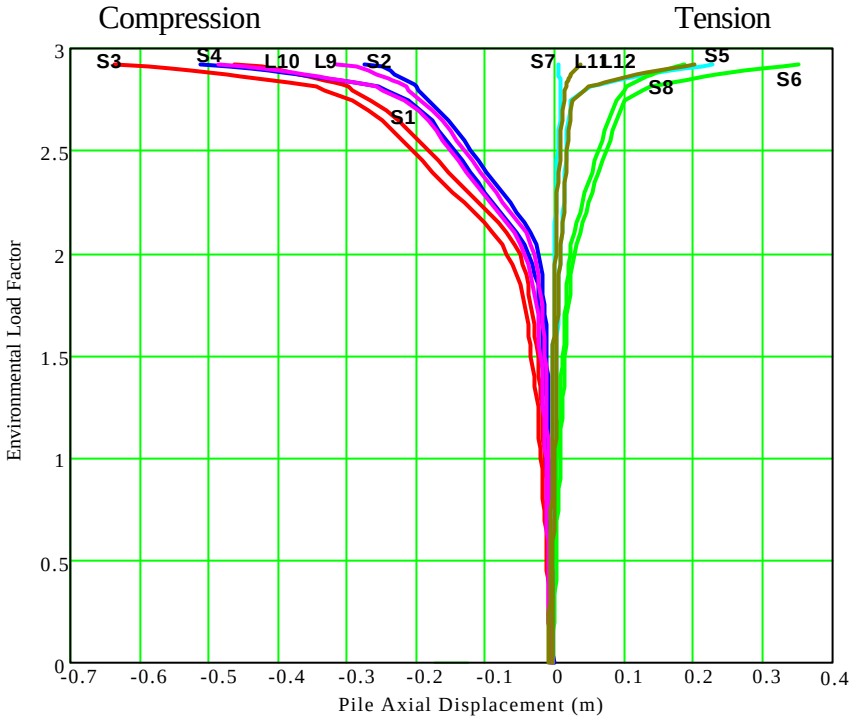

Figure 21 **Undegraded foundation system: axial pile deflection vs. environmental load factor**

Pile Arrangement

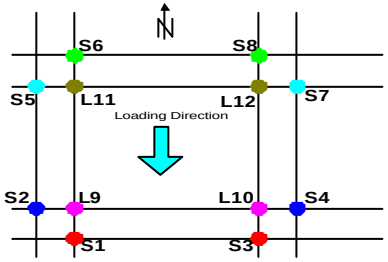

7. MODELLING OF STORMS

The modelling of the long-term storm characteristics requires models for long term statistics and short term statistics.

The short term storm model describes the wave statistics given that the storm is of a given peak intensity. A storm is characterised by its peak intensity (peak significant wave height) H_{smax}, and by the storm profile given in the draft ISO recommendations [7].

The long term statistics describe the annual probability that storms of a given peak intensity are exceeded. The long term statistics are defined in terms of a probability distribution for peak storm intensity.

7.1 Notation

H	Individual wave height
H_s	Significant wave height, Sea-State Intensity
H_{max}	Maximum wave height in a sea state
H_{smax}	Maximum sea-state intensity of largest annual storm.
T	Individual wave period
T_z	Mean Up-Crossing Period
T_p	Period corresponding to spectral peak
T_m	Mean Wave Period
T_{state}	Duration of sea state
N	Number of waves in a particular sea-state

The following relationships between sea state intensity *Hs*, and peak spectral period, T_p, and mean upcrossing period, T_z, are used:

$T_p = 0.4392\text{Hs} + 6.0192$

$T_z = 0.3988\text{Hs} + 9.5341$

The intensity of a sea state is expressed in terms of the significant wave height, H_s. As a storm progresses, the instantaneous value of H_s changes, reaching a peak and then decaying. The Draft ISO [7] recommends the profile for storm build-up in the North Sea shown in Figure 22.

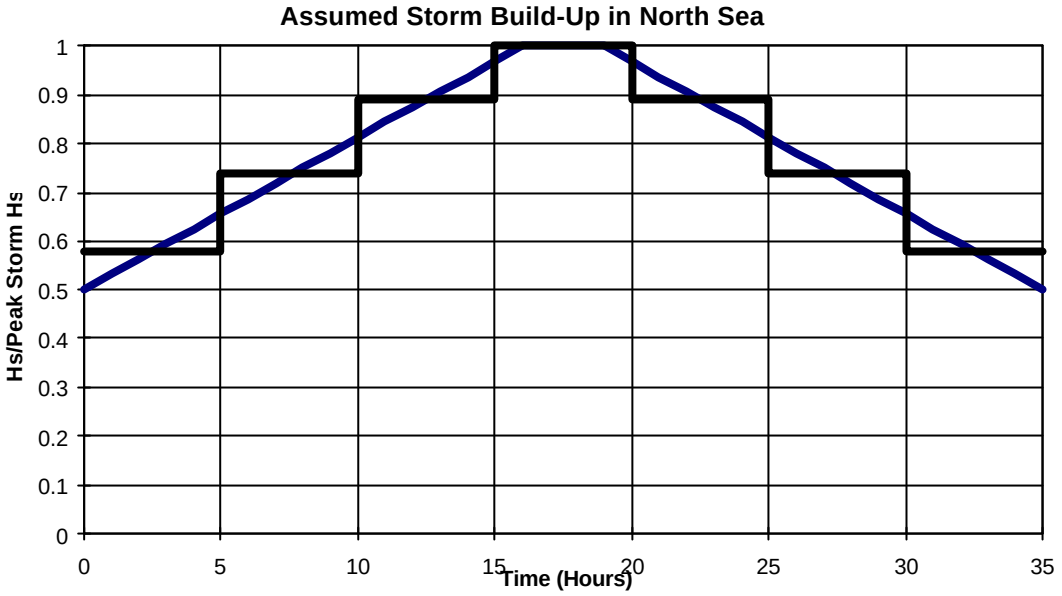

Figure 22 Storm history

In the present study, the full storm history was divided into a series of individual sea states of constant H_s within which the sea statistics were assumed to be stationary.

7.2 Long term storm statistics

The long term storm statistics define the probability of occurrence of the largest storm within a given time period, normally one year. The storm peak intensity may be used as the random parameter, with all other parameters being dependent on this value. For the wave from North condition at the Central North Sea site, the probability distribution for peak storm H_s was inferred from the data provided which gave maximum 1 year, 10 year 50 year and 100 year H_s values. Assuming these to be representative of maximum storm H_s, the distribution of the peak H_s of the largest storm can be taken to be a Gumbel distribution with parameters:

$\alpha = 1.143\ m^{-1}$

$u = 7.425\ m$

7.3 Short term storm statistics

The storm was divided into a number of constant sea-state blocks, each of duration T_{state}. The mean up-crossing period, T_z was used to estimate the number of waves in the sea-state:

$$N = T_{state} / T_z$$

7.3.1 Individual wave height distribution

For the type of narrow-banded sea state to be expected in the central North Sea. The probability density function of individual wave height, H, for a given sea state characterised by H_s, the wave height was modelled using a Rayleigh distribution, given by:

$$f_{H|Hs}(h|h_s) = 2\left(\frac{1.416}{h_s}\right)^2 h \exp\left(-\left(1.416\frac{h}{h_s}\right)^2\right) \quad (12)$$

The period associated with a particular wave height was estimated from the modal value of the Longuet-Higgins joint wave height/wave period distribution.

7.3.2 Distribution of maximum wave in a sea-state

The maximum wave height occurring in a given sea state is denoted H_{max}. It is a function of the number of waves occurring in the sea state, and has a cumulative distribution function given by

$$F_{H_{\max}}(h_{\max}) = \left[F_H(h)\right]^N \quad (13)$$

where N is the expected number of waves in the seastate. The most common measure of the extreme wave is the modal value of the distribution of the maximum wave, H_{max}. The typical relationship between the individual wave distribution and distribution of the maximum wave in the sea-state is shown in Figure 23.

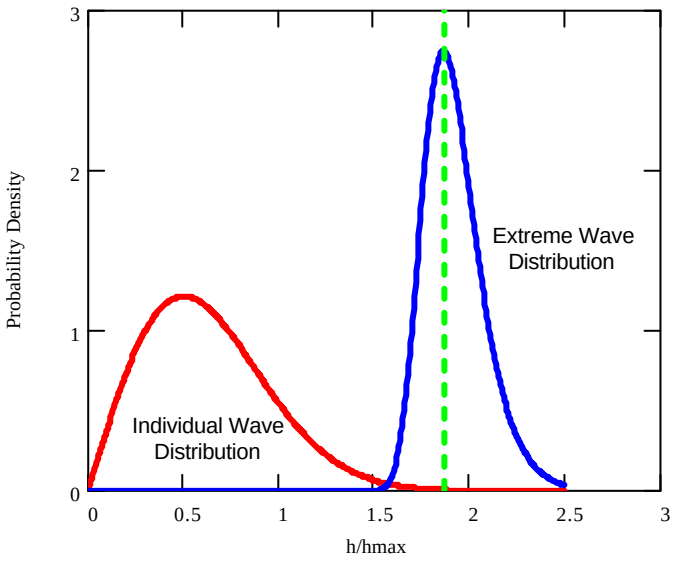

Figure 23 Short-term wave statistics in a sea-state

7.3.3 Distribution of maximum wave in a storm

The distribution of the maximum wave in a storm is the product of the distributions of the maximum wave within each sea-state.

$$F_{H_{\max}}\left(h_{\max}\right) = \prod_{i=1}^{7}\left(F_{H|H_{si}}\left(h\right)\right)^{N_i} \tag{14}$$

The distribution of the maximum wave in a storm calculated according to Equation (14) has been fitted to a Gumbel distribution and is tabulated, for storms of different return periods, in Table 4.

Table 4 Gumbel distribution parameters for maximum wave in storm

Storm Return Period T **[Years]**	**Maximum Storm Intensity** H_{smax} **[m]**	**Distribution of Maximum Wave In Storm ($H_{max}\|S_T$)**			
		$a_{H_s\|S_T}$ **[m^{-1}]**	$u_{H_s\|S_T}$ **[m]**	$m_{H_s\|S_T}$ **[m]**	cov $H_s\|S_T$
1	8.5	0.98	15.9	16.5	0.08
10	11.1	0.75	20.6	21.4	0.08
50	12.9	0.64	23.9	24.8	0.08
100	13.8	0.60	25.5	26.5	0.08
500	15.6	0.53	28.8	29.9	0.08
1000	16.4	0.51	30.2	31.4	0.08
5000	18.2	0.46	33.4	34.7	0.08
10000	19.0	0.44	34.9	36.2	0.08
50000	20.8	0.40	38.1	39.5	0.08

8. ANALYSIS OF FOUNDATION CAPACITY DEGRADATION FOR EXAMPLE NORTH SEA PLATFORM

8.1 Procedure for degradation analysis

The procedure that was used for the analysis of the degradation arising in the platform during a given storm history is depicted in the flow chart of Figure 24. The method adopted accounts for both the effects of the redistribution in soil strength within a pile and the progressive redistribution in loading between piles as the storm history progresses and changes in relative pile stiffness occurs. The structural capacity calculations are based on the unaged 50 day soil strength. This contrasts with the calibration check which allowed implicitly for ageing in the field tests.

The model for cyclic t-z spring response and degradation developed for the isolated pile analysis, described in Section 4, above was adopted for the axial pile response. In addition to this, a model for the lateral response was used according to the API 20th Edition [6] recommendations for p-y soil springs. The parameters used for the soil model were

f' = 37^o in dense sand at depths greater than 10m below mudline

f' = 34^o in medium dense sand at depths less than 10m below mudline

$g' = 9.7\ kN/m^3$

A hysteretic behaviour was adopted for the p-y curves. The initial non-linear p-y response given in the API 20th Edition recommendations was assumed until first unloading was encountered. Following the first unloading event, each p-y curve was assumed to take on a bi-linear hysteretic characteristic similar to that of the t-z curves. The p-y and t-z hysteretic cyclic spring formulation, and the degradation model were programmed into the RASOS software which was used for the analysis of the degradation of the pile system.

The analysis procedure for a storm started with the initial undegraded soil properties. Starting from the first sea-state and the smallest wave block amplitude within the sea state, the wave was passed through the platform and the sequence of structural loading as the wave travels through the platform was obtained. This loading was applied incrementally in a non-linear analysis of the complete pile system. The structure was assumed to remain elastic throughout the process. A total of three wave cycles were passed through the structure to ensure that the cyclic response reached a steady state. The maximum and minimum forces arising in the t-z springs were extracted and used to evaluate the cyclic and average components of the shaft shear stress, which were then used along with the number of waves of that amplitude to evaluate the degraded capacity. The capacity and stiffness of each t-z spring was then updated accordingly and the next block of waves applied to the structure. The procedure was repeated until the complete storm had been analysed.

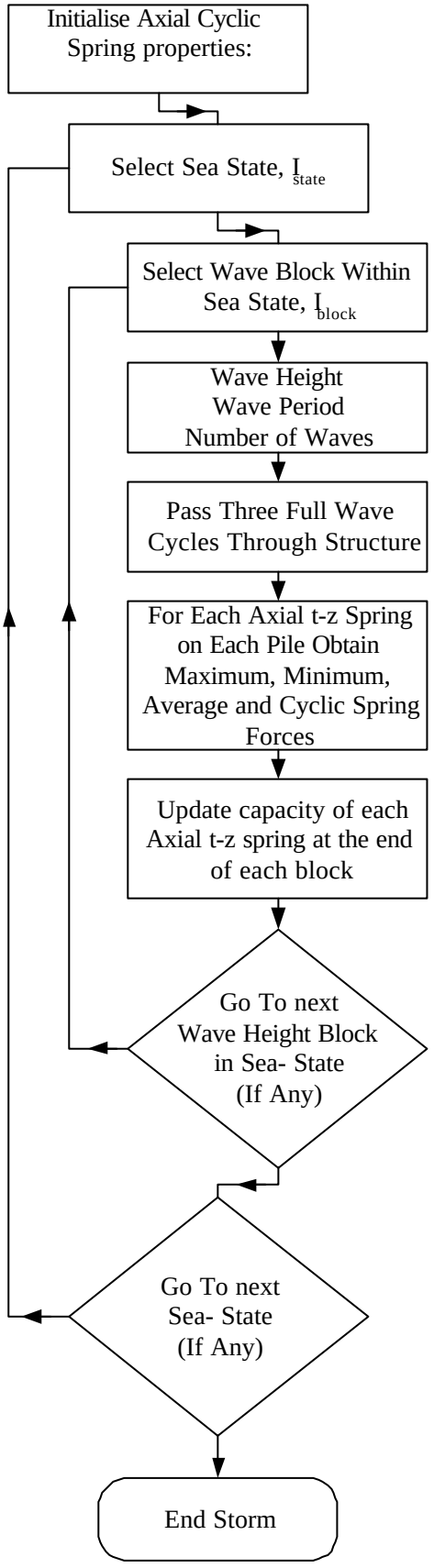

Figure 24 Flow chart of full storm degradation analysis

The analysis of degradation for these storms assumed that the storm history was divided into seven constant intensity sea-states each of 5 hours duration. The Rayleigh distribution for individual wave height was used to evaluate 5 blocks of waves per sea-state. These are given in Table 5 for the 100 year storm and Table 6 for the 1000 year storm.

In this analysis, the cyclic degradation model was assumed to be acting irrespective of the amplitude of the wave. The interaction between cyclic degradation and ageing is thus being ignored. This effect is considered in the simplified treatment using the loading threshold in the subsequent analysis. The applied range of cyclic loading are not necessarily very severe in relation to the static capacity.

Table 5 100 year storm discretisation. Number of waves in each block for each sea-state

Wave Height (m)	Wave Period (s)	Sea State Number						
		1	2	3	4	5	6	7
2.6	8.3	805	534	375	295	375	534	805
7.8	13.7	560	621	573	516	573	621	560
13	15	47	154	248	291	248	154	47
18.2	15.4	0	12	45	80	45	12	0
23.4	15.6	0	0	3	11	3	0	0

Table 6 1000 year storm discretisation. Number of waves in each block for each sea-state

Wave Height (m)	Wave Period (s)	Sea State Number						
		1	2	3	4	5	6	7
3.1	8.9	764	502	349	274	349	502	764
9.2	14.6	538	588	538	481	538	588	538
15.4	16	47	148	235	274	235	148	47
21.5	16.5	0	12	44	76	44	12	0
27.7	16.7	0	0	3	11	3	0	0

8.2 Degradation analysis results

The full model for degradation of the pile system was used to estimate the loss in structural capacity during the 100 and 1000 year return period storms. The collapse event during a storm was assumed to be the result of degradation in capacity followed by an extreme wave event sufficiently large to collapse the platform. The capacity halfway through the storm was

considered to provide a measure of the resistance of the platform to the collapse wave event.

For the 100 year storm, the amplitude of the total axial force down the pile is shown in Figure 25. The progressive degradation throughout the history of the 100 year return period storm is shown in Figure 26. Similarly the axial cyclic force amplitude and the progressive pile deterioration during the 1000 year return period storm are illustrated in Figure 27 and Figure 28 respectively.

It can be seen from the plots of axial cyclic amplitude that the outer-most skirt piles attracted the greatest loading. For the largest waves in the 100 year storm this was 9.5 MN, corresponding to 22% of the compressive shaft capacity and 28% of the tensile shaft capacity. In the 1000 year storm, the largest waves transferred a cyclic load amplitude of 13 MN to the outer skirt piles, corresponding to 28% of the original compressive shaft capacity and 38% of the original tensile shaft capacity. This was superimposed onto the compressive vertical loading condition which ranged between 18 MN and 10 MN for the outer skirt piles.

The pile axial loading arising from waves of the same height can be seen to have decreased in the outer skirt piles and increased in the inner skirt and leg piles as the storm progressed. This behaviour arose as a result of the relative changes in pile stiffness with degradation. For the largest wave in the three most intense sea-states, the cyclic force amplitude in the outermost piles decreased by 6%.

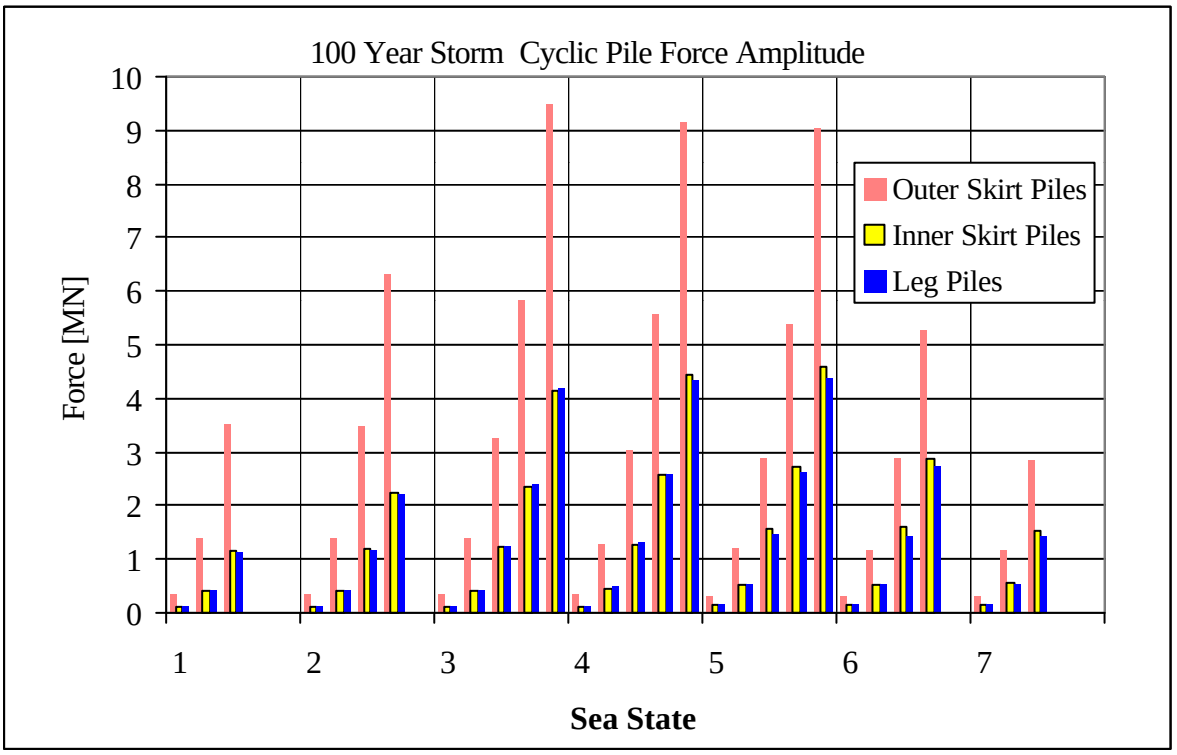

Figure 25 100 year storm, full degradation model, amplitude of cyclic pile force amplitude

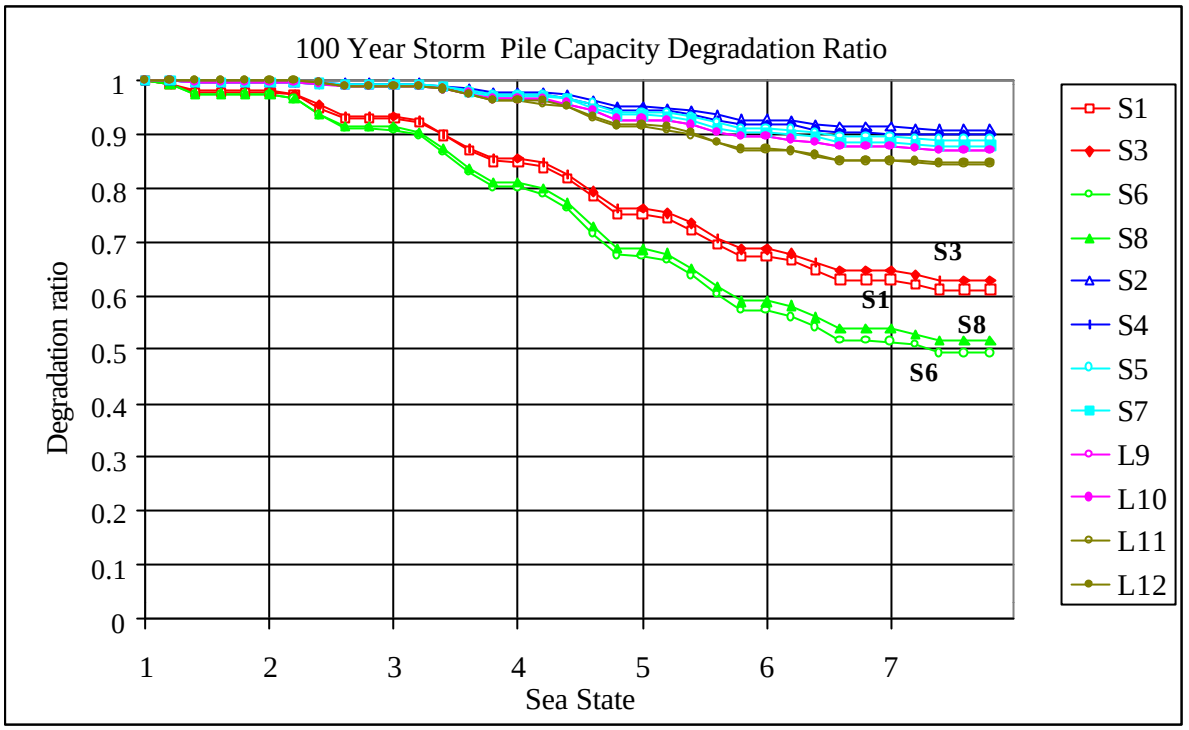

Figure 26 100 year storm, full degradation model, pile axial capacity degradation history

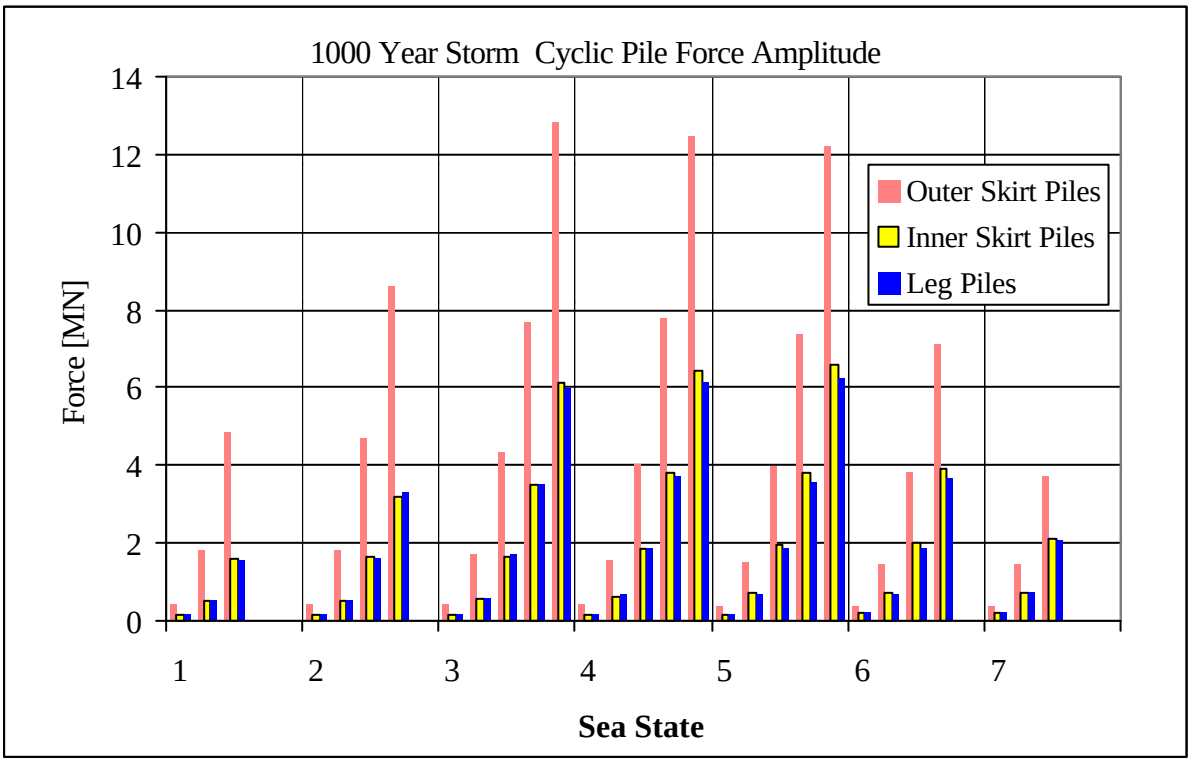

Figure 27 1000 year storm, full degradation model, amplitude of cyclic pile force amplitude

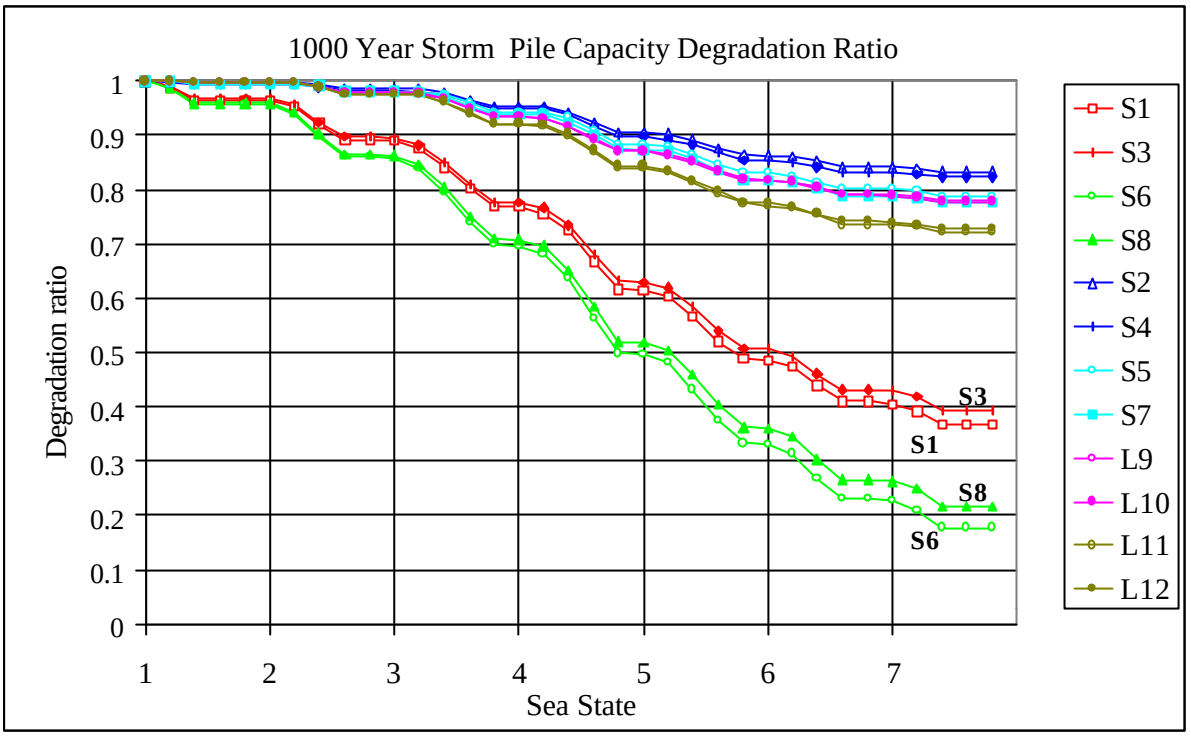

Figure 28 1000 year storm, full degradation model, pile axial capacity degradation history

A summary of the pile degradation during the storm is presented in Table 7. The degradation at the end of the storm and at the middle of the storm is given for the three pile types. The greatest degradation occurred in the outer skirt piles, which lost 32% of their tensile capacity at the middle of the 100 year storm and 50% of their capacity by the end of the 100 year storm. In the 1000 year storm, the same piles lost 50% of their tensile capacity by the middle of the storm and 82% by the end of the storm. The compressive capacity degradation was less pronounced since the tip capacity, originally some 25% of the total, did not degrade. The capacity of the other piles degraded by considerably less.

Table 7 Individual pile capacity degradation

	100 Year Storm				**1000 Year Storm**			
	Middle of Storm		End of Storm		Middle of Storm		End of Storm	
	Comp.	Tens.	Comp.	Tens.	Comp.	Tens.	Comp.	Tens.
Outer Skirt Pile	**25%**	**32%**	**39%**	**50%**	**38%**	**50%**	**63%**	**82%**
Inner Skirt Pile	**5%**	**6%**	**9%**	**12%**	**10%**	**12%**	**18%**	**21%**
Leg Piles	**7%**	**9%**	**13%**	**16%**	**13%**	**16%**	**22%**	**28%**

The degradation in the capacity of the foundation system was assessed by performing pushover analyses using the approach described in Section 6. The 100 year return period environmental load was used as the reference design loading for determining the RSR for the full foundation system. Load-deflection plots are shown for the degraded system in the middle of the 100 and 1000 year return period storms in Figure 29 and Figure 30 respectively. The individual pile axial forces and pile-head axial deflections computed during the course of the pushover analyses are shown in Figure 31 and Figure 32 respectively for the middle of the 100 year return period storm, and in Figure 33 and Figure 34 for the middle of the 1000 year storm.

In both cases, the overall pattern of failure is similar to that for the undegraded system. The main differences are that the outer skirt piles have a considerably reduced shaft friction capacity.

Table 8 gives the environmental load factor for first pile component failure and the system-based RSR at the middle and at the end of the two storms. It can be seen that the system capacity at the middle of the 100 year storm reduced by 17%, whereas the component failure load factor reduced by 24%.

The reduction in component failure load factor was less than the degradation in the actual capacity of the pile; 24% compared with 32%. This is because the critical failure component, pile S6 failing in tension, was initially in compression due to the initial vertical loading. Part of the environmental loading was required to overcome this dead loading.

The critical component was pile S6 failing in tension, whereas the design was critical for pile S1 failing in compression. As a result of the redistribution that occurred once the compressive shaft friction resistance was overcome, pile S6 attracted less load and was thus, in a way, "protected" against complete tip failure by its sudden loss in stiffness. This was a feature of the pile system, and for non-redundant foundation systems, for example four legged Jackets, redistribution cannot occur, and failure will most likely be governed by the compressive pile failure. In such a case the RSR is likely to be very close to the first component failure load factor. Degradation is expected to have an effect on the RSR close to that on the individual pile capacity, i.e., of 15% at the middle of the storm.

Table 8 Degradation in foundation capacity

	Middle of Storm		**End of Storm**	
	Component Failure Factor	**System RSR**	**Component Failure Factor**	**System RSR**
Undegraded Structure	**1.90**	**2.95**	**1.90**	**2.95**
100 Year Storm	**1.45** **24%**	**2.45** **17%**	**1.10** **42%**	**2.20** **25%**
1000 Year Storm	**1.20** **37%**	**2.20** **25%**	**0.70** **63%**	**1.75** **41%**

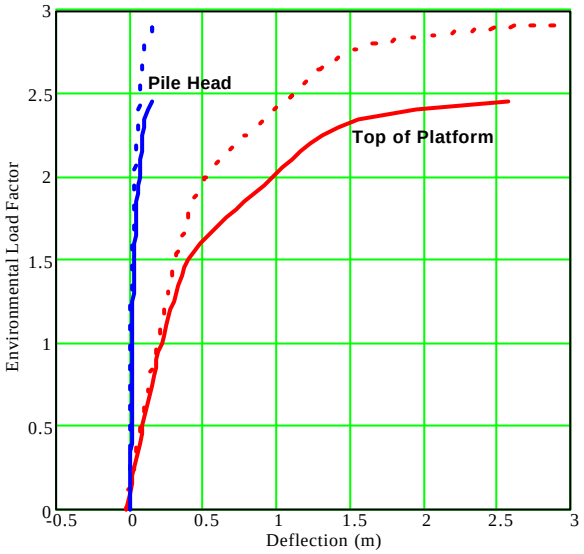

Figure 29 Pushover analysis for degradation in middle of 100 year storm

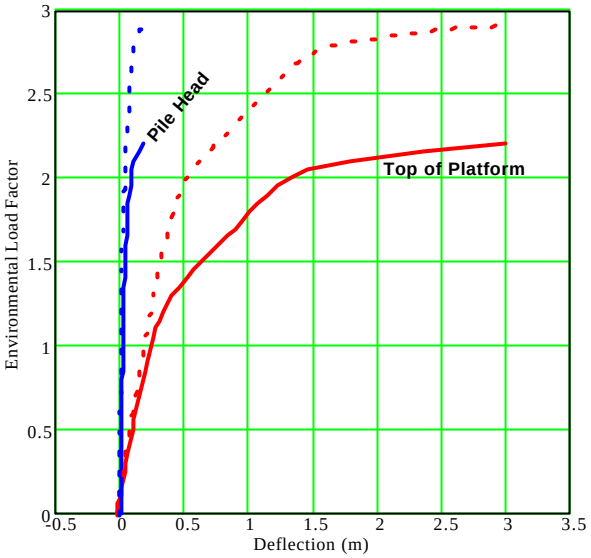

Figure 30 Pushover analysis for degradation in middle of 1000 year storm

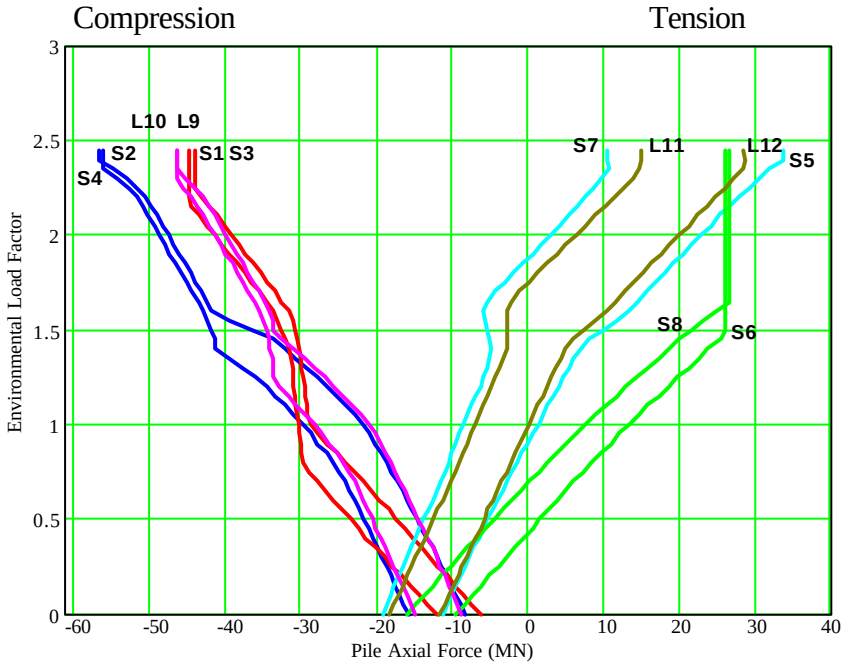

Figure 31 Middle of 100 Year Storm: Axial Pile Load vs. Environmental Load Factor

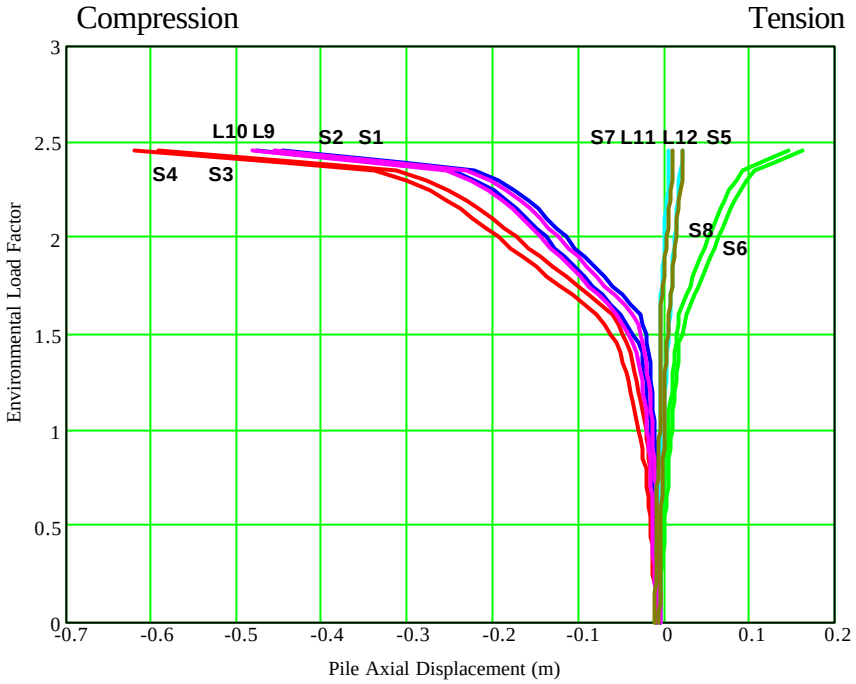

Figure 32 Middle of 100 Year Storm: Axial Pile Deflection vs. Environmental Load Factor

Pile Arrangement

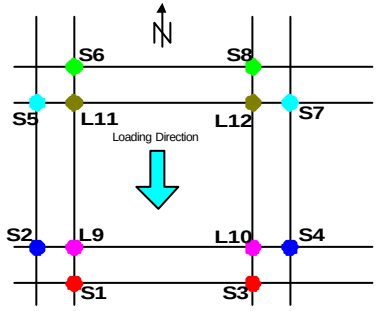

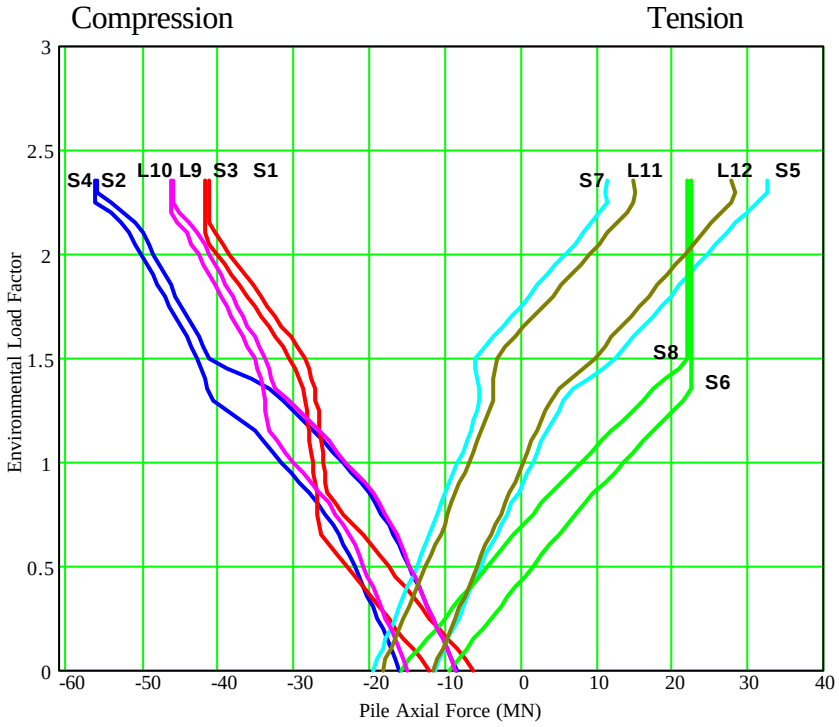

Figure 33 **Middle of 1000 year storm: axial pile load vs. environmental load factor**

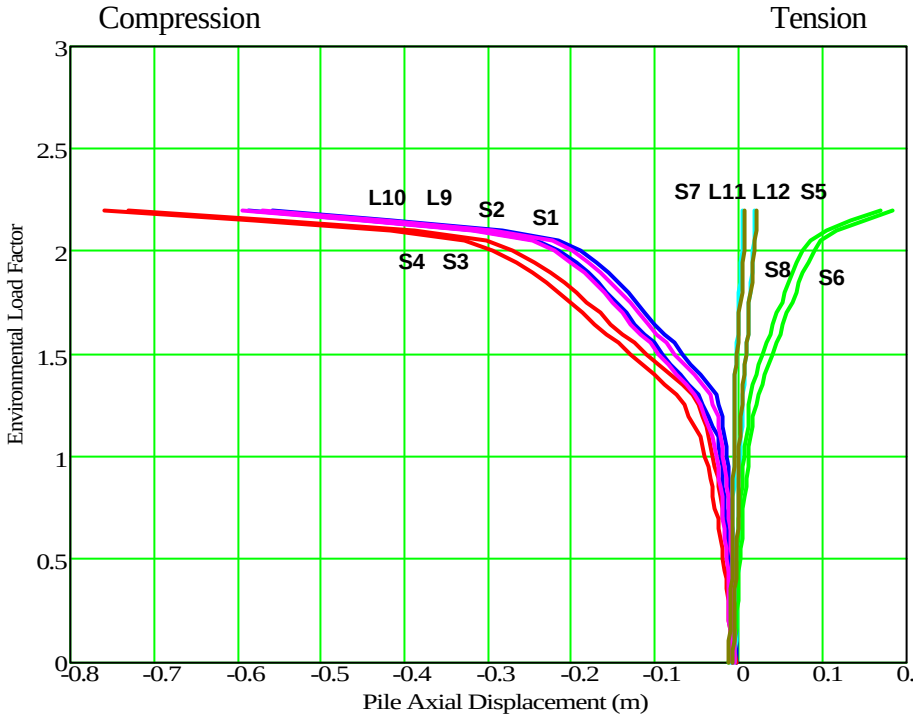

Figure 34 **Middle of 1000 year storm: axial pile deflection vs. environmental load factor**

Pile Arrangement

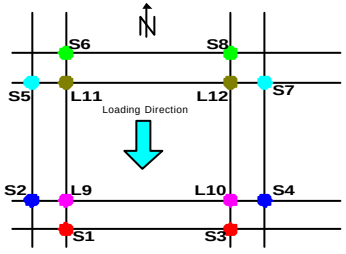

9. REANALYSIS FOR DEGRADATION THRESHOLD MODEL

The full degradation model used for the above analyses assumed that all the waves impinging the structure during a storm contributed to the degradation of the shaft frictional resistance. The experiments by Jardine [1] showed that small amplitude cycles have the effect of increasing the rate of ageing resulting in an increase in the shaft capacity. Changes in pile skin friction capacity are therefore a combination of gain in strength in those parts of the pile subjected to low amplitude cycling, and degradation in strength in those parts of the pile where the local cyclic shear stress amplitude is high. In the absence of an appropriate model for local increase and degradation of pile strength, it was decided, after discussion with Jardine, to obtain an approximate threshold for the cyclic component of the total pile axial force below which no capacity degradation occurs and above which the full degradation model used above was to be implemented.

The threshold for the cyclic axial loading component was determined by considering an equivalent threshold obtained from the full scale experiments at Dunkirk. An analysis was performed on the test pile using the Mathcad spreadsheet.

Jardine's experiments showed that the static capacity of a 19.4 m long Dunkirk pile degraded when P_{cyc}/P_{max} was above 0.3 times of the original tensile shaft capacity, but showed enhanced ageing when P_{cyc}/P_{max} was below 0.2 times the original tensile shaft capacity. Here P_{cyc} is the axial cyclic loading component and P_{max} is the total tensile pile capacity. On the basis of these results it was decided that, for the Dunkirk pile, the value of P_{cyc}/P_{max} below which no degradation occurs was 0.25 times the original tensile capacity.

The percentage of tensile capacity degradation predicted by the Mathcad spreadsheet is plotted as a function of P_{cyc}/P_{max} for the Dunkirk test pile and for the synthetic leg and skirt piles in Figure 35. All piles where subjected to 1000 constant amplitude cycles. The threshold value of P_{cyc}/P_{max} for the synthetic piles was derived on the assumption that the percentage degradation predicted by the Mathcad spreadsheet for the threshold value of P_{cyc}/P_{max} for Dunkirk pile is equal to that predicted for the Skirt and Leg piles at their threshold values of P_{cyc}/P_{max}. It can be seen from Figure 35 that the model predicted 22% degradation for the Dunkirk pile at the end of the 1000 cycles at the threshold value of P_{cyc}/P_{max} of 0.25. The synthetic piles both gave this level of degradation for P_{cyc}/P_{max} equal to 0.2. Thus, the threshold value of P_{cyc}/P_{max} below which it was assumed that no degradation would take place, was taken to be 0.2.

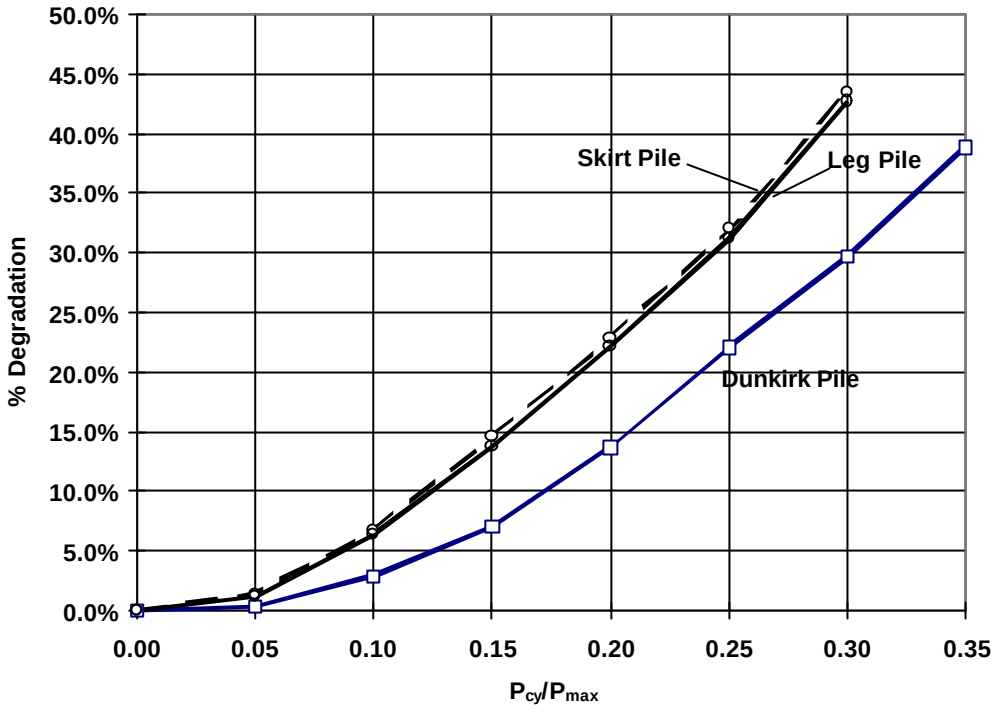

Figure 35 Relationship between cyclic load amplitude and degradation after 1000 cycles as predicted by the degradation model

It was seen from the full degradation analysis that the axial cyclic load component of the force attracted by the piles changed for the same wave height as the cyclic load history progressed. The outer skirt piles attracted smaller load and the inner skirt piles and leg piles attracted greater load as the outer piles lost stiffness relative to the inner piles as the storm progressed. For the maximum wave occurring in sea-states 3, 4 and 5, this reduction was of the order of 6% for the 100 year wave history. For the reanalysis of the system using the threshold model, it was assumed that this redistribution does not occur, and that the pile forces induced by a given wave height do not change as a consequence of pile degradation. On this basis, the threshold cyclic force component and wave heights for the outer and inner leg piles, and the leg piles were calculated and are tabulated in Table 9 below.

Table 9 Threshold cyclic axial load and wave height

	Threshold Cyclic Axial Force Component [MN]	**Threshold Wave Height [m]**
Outer Skirt Piles	6.8	19.2
Inner Skirt Piles	6.8	29.2
Leg Piles	5.8	27.1

A rediscretisation of the 100 year and 1000 year storms was carried out in order to ensure that the waves above the threshold wave height were sufficiently well represented. The selected wave blocks for the 100 year storm are tabulated in Table 10. The modal value of the maximum wave in the 100 year storm does not exceed the degradation threshold for the leg and skirt piles. The wave blocks for the outer skirt pile wave blocks of the 1000 year storm are given in Table 11, and those for the leg piles in Table 12. The modal maximum wave in the 1000 year storm will not cause degradation in the inner skirt piles.

The degradation in pile capacity calculated using this approach are depicted in Figure 36 and Figure 37.

Table 10 Analysis with degradation threshold: wave discretisation, 100 year storm, outer skirt piles

		Sea State Number				
Wave Height (m)	**Cyclic Axial Force (MN)**	**2**	**3**	**4**	**5**	**6**
19.5	7.0	**1**	**11**	**24**	**11**	**1**
22.1	8.7	**0**	**3**	**8**	**3**	**0**
25.0	10.6	**0**	**0**	**2**	**0**	**0**

Table 11 Analysis with degradation threshold: wave discretisation, 1000 year storm, outer skirt piles

		Sea State Number				
Wave Height (m)	**Cyclic Axial Force (MN)**	**2**	**3**	**4**	**5**	**6**
20.6	7.7	**6**	**25**	**43**	**25**	**6**
23.5	9.7	**1**	**8**	**19**	**8**	**1**
26.4	11.9	**0**	**2**	**7**	**2**	**0**
29.2	14.3	**0**	**0**	**2**	**0**	**0**

Table 12 Analysis with degradation threshold: wave discretisation: 1000 year storm, leg piles

		Sea State Number				
Wave Height (m)	**Cyclic Axial Force (MN)**	**2**	**3**	**4**	**5**	**6**
28.9	7.0	**0**	**1**	**4**	**1**	**0**

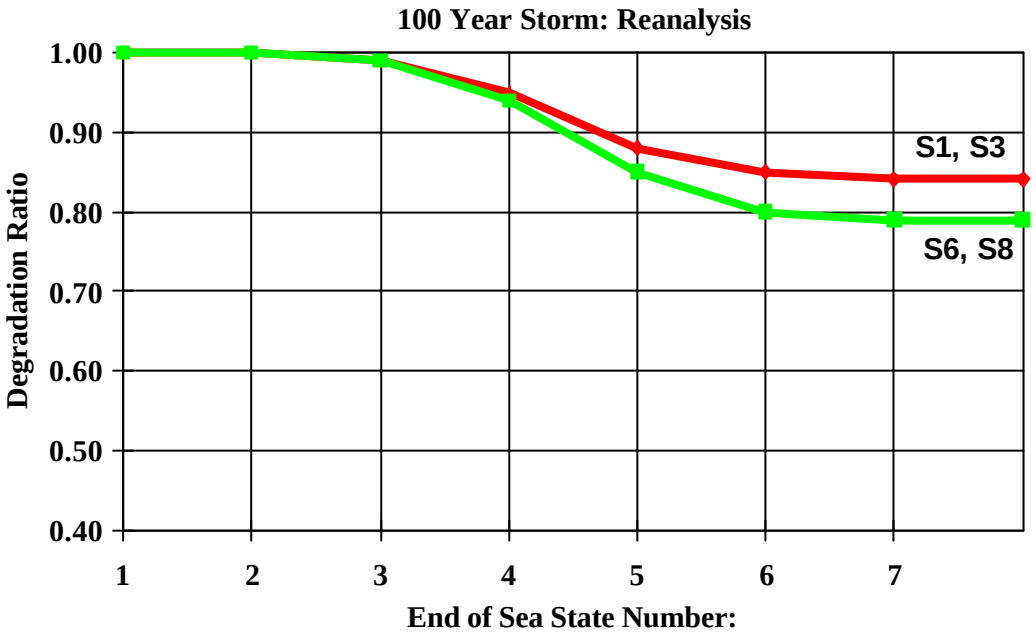

Figure 36 Analysis with degradation threshold: 100 year storm. Pile degradation history

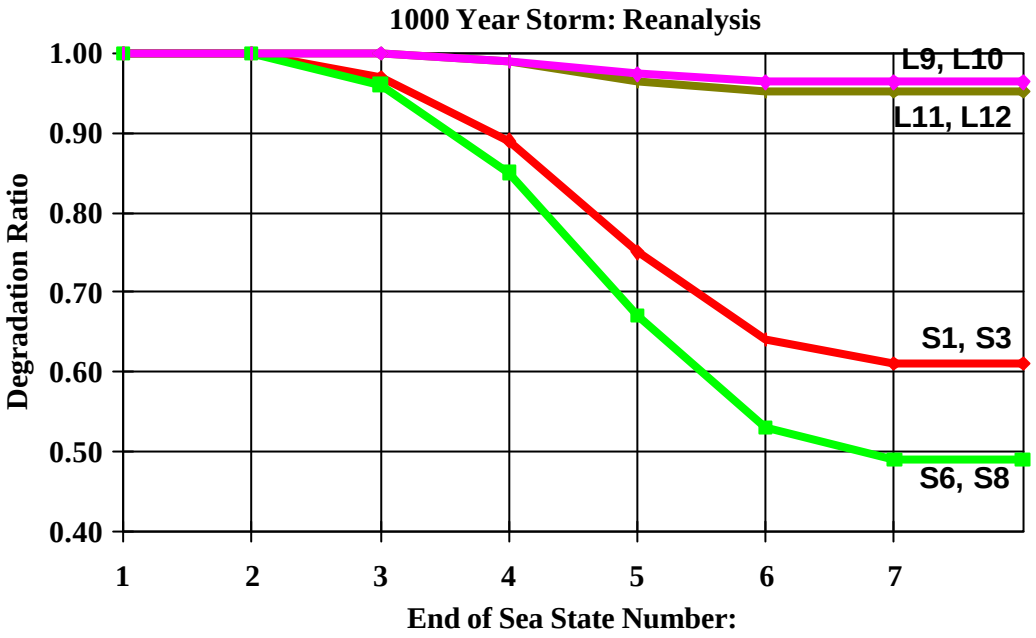

Figure 37 Analysis with degradation threshold: 1000 year storm. Pile degradation history

Table 13 Analysis with degradation threshold. Individual pile capacity degradation

	100 Year Storm				1000 Year Storm			
	Middle of Storm		End of Storm		Middle of Storm		End of Storm	
	Comp.	Tens.	Comp.	Tens.	Comp.	Tens.	Comp.	Tens.
Outer Skirt Pile	12%	15%	16%	21%	25%	33%	39%	49%
Inner Skirt Pile	0%	0%	0%	0%	3%	4%	4%	5%
Leg Piles	0%	0%	0%	0%	0%	0%	0%	0%

Individual pile capacity degradation for the analysis with the degradation threshold is given in Table 13. The outer skirt piles suffered the most significant degradation, with a maximum 15% loss in tensile shaft capacity after sea-state 4 for the 100 year storm, and 33% loss in tensile capacity for the 1000 year storm.

Individual degraded soil t-z spring capacity and stiffness parameters were output by the Mathcad spreadsheet at the end of sea-state four and at the end of the storm. These were then read in by the RASOS program and used for pushover analyses in order to obtain the

foundation system RSR. The RSR and environmental factor at first pile failure obtained from these analyses are tabulated in Table 14.

Table 14 Threshold analysis: degradation in reserve strength ratio

	Middle of Storm		End of Storm	
	Component Failure Factor	**System RSR**	**Component Failure Factor**	**System RSR**
Undegraded Structure	**1.90**	**2.95**	**1.90**	**2.95**
100 Year Storm	**1.75** **8%**	**2.80** **5%**	**1.65** **13%**	**2.70** **9%**
1000 Year Storm	**1.50** **21%**	**2.55** **14%**	**1.25** **34%**	**2.40** **19%**

The results for the analysis with the degradation threshold obviously showed considerably less overall degradation than the full degradation model. At the middle of the 100 year storm, i.e. after sea-state 4, the worst degradation of 15% was seen in the outer skirt pile. For the 1000 year storm the degradation in the outer skirt pile at the middle of the storm was 33%.

The degradation in component failure capacity was 8% at the middle of the 100 year storm and 21% at the middle of the 1000 year storm. This is considerably lower than the individual pile capacity degradation, and was a result of the initial compressive dead loading and the redistribution following exhaustion of the compressive shaft friction capacity, factors already described in the discussion on the full degradation model results.

The degradation in system capacity was 5% for the 100 year storm and 14% for the 1000 year storm. The degradation in system capacity observed in the 100 year storm is thus small. Again this is a reflection of the enhanced strength of the platform arising from system effects. The inner skirt piles and the leg piles showed no degradation at all during the 100 year storm, and very little degradation during the 1000 year storm. However their strength needed to be mobilised for full foundation collapse.

10. CALCULATION OF PROBABILITY OF COLLAPSE

10.1 Conditional probability of failure during a storm

During a storm a platform is subjected to a sequence of waves of varying amplitude, period and direction. Moreover other environmental parameters such as current and wind also affect the platform and also vary in magnitude and direction.

For the platform to collapse during the course of a storm it must, at some point, experience environmental forces sufficiently high to exceed its capacity. If wave-induced degradation of the foundation capacity occurs, then the platform capacity at a given instant in time is a non-stationary stochastic process which is a function of the random wave history up to that instant. Similarly, the platform loading is also a non-stationary random process. The safety margin $M(t)$ at any instant in time t is:

$$M(t) = \lambda_R R(t) - B_F F(t) \tag{15}$$

where $R(t)$ is the random platform base-shear capacity at time t during the storm, λ_R is a time-independent random variable representing the resistance uncertainty, $F(t)$ is the total force on the platform at time t and B_F is a time-independent random variable representing the uncertainty in modelling the environmental loading on the jacket. The probability of failure during a storm is thus the probability that the safety margin $M(t)$ is smaller than zero at any instant during the storm. This may be written as:

$$P_f = P\left[\bigcup_{0<t<t_{Storm}} \left(\lambda_R R(t) - B_F F(t) < 0\right)\right] \tag{16}$$

The task of evaluating this expression is not trivial and considering the nature of the physical degradation model, a simplified approach was adopted.

If the foundation capacity degrades continuously throughout the storm (i.e. $R(t)$ is a monotonically decreasing function of t), then Equation (16) is equivalent to:

$$P_f = P\left[\bigcup_{0<t<t_{Storm}} \left(\lambda_R R(t) - B_F F\left(\max_{t>t}\left(H(t)\right)\right) < 0\right)\right] = P\left[\bigcup_{0<t<t_{Storm}} \left(M'(t) < 0\right)\right] \tag{17}$$

where the force component is now that induced by the wave of maximum height following instant t.

The probability of failure given by Equation (17) is expressed in terms of the union of an infinite number of failure events given in terms of a continuous variable t. However the safety margin $M'(t)$ is expected to have high autocorrelation over a long period of time. Under these conditions, an appropriate approximation for the failure probability in a given storm is:

$$P_f \approx \max_{0<t<t_{storm}} \left[P\left[\lambda_R R(t) - B_F F\left(\max_{\tau>t}\left(H(\tau)\right)\right) < 0\right]\right] = \max_{0<t<t_{storm}} \left[P\left[M'(t) < 0\right]\right] \tag{18}$$

The instant at which the maximum probability value of Equation (18) occurs is approximately the same point at which the safety margin *M'(t)* takes on its minimum value. Figure 38 shows the system capacity degradation, the most likely maximum force and the safety margin *M'(t)* at the end of each sea state of the 100 year storm. All three quantities have been normalised to unity at the start of the storm. The safety margin can be seen to reach a minimum value in sea state 4.

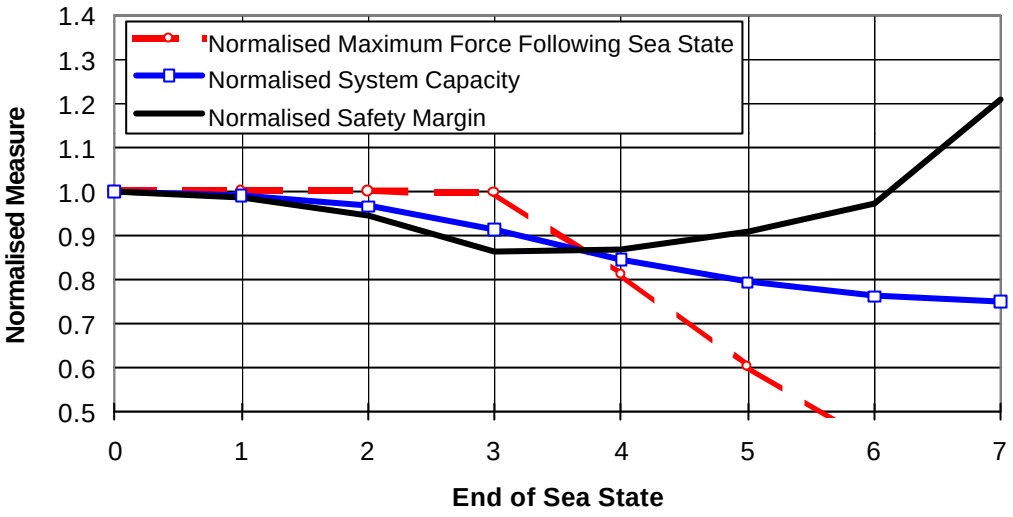

Figure 38 Normalised degradation, force and RSR for full degradation model during 100 year storm

On the basis of this analysis, the point in the storm which is most critical with regards to the safety of the platform was taken to be at the end of sea-state 4. In calculating the conditional probability of failure for a given storm, the wave height distribution was taken to be that of the maximum wave in the whole storm. Gumbel fit parameters for the complete storm H_{max} have been given in Table 4. The force model uncertainty parameter B_F was taken to be lognormal with a median of 1 and a cov of 0.15. The random resistance parameter l_R was taken to be lognormal with a median of 1 and a cov of 0.25.

The conditional probability of failure given a storm is calculated using the conditional short-term H_{max} distribution parameters given in Table 4 and using the First Order Reliability Method implemented in RASOS.

The conditional probability of platform failure probability for the 100 and 1000 year storms is tabulated in Table 15. Three failure criteria were considered: First component failure, system failure and failure assuming that the system degradation was equal to the degradation in the most degraded pile. This last criterion gives an indication of the effects of degradation on the reliability of non-redundant foundations where the environmental loading is large compared with the dead load effects, and for which foundation failure is governed by tensile pile failure. It has been included here in order to estimate the influence of degradation on platforms with non-redundant foundation systems.

Table 15 Conditional probabilities of component and system collapse

	Degradation Model Type	Deterministic Environmental Load Factor			Conditional Failure Probability		
		Component	System	System degradation equals maximum pile degradation	Component	System	System degradation equals maximum pile degradation
100 Year Storm	Undegraded Structure	**1.90**	**2.95**	**2.95**	**1.8×10^{-2}**	**3.5×10^{-4}**	**3.5×10^{-4}**
	Full Degradation	**1.45**	**2.45**	**2.00**	**1.0×10^{-1}**	**2.1×10^{-3}**	**2.5×10^{-2}**
	Analysis with Threshold	**1.75**	**2.80**	**2.51**	**3.1×10^{-2}**	**5.8×10^{-4}**	**6.0×10^{-3}**
1000 Year Storm	Undegraded Structure	**1.90**	**2.95**	**2.95**	**1.4×10^{-1}**	**7.3×10^{-3}**	**7.3×10^{-3}**
	Full Degradation	**1.20**	**2.20**	**1.48**	**6.8×10^{-1}**	**6.7×10^{-2}**	**5.3×10^{-1}**
	Analysis with Threshold	**1.50**	**2.60**	**1.98**	**3.8×10^{-1}**	**2.0×10^{-2}**	**2.5×10^{-1}**

10.2 Annual probability of failure for all possible storms

In order to estimate the total annual probability of failure, it is necessary to consider the possibility of failure over all possible storms. The annual probability of collapse may be calculated from conditional probabilities of collapse for storms of given return period T from the following expression:

$$P(F) = \int_0^\infty P(F \mid S_T) \frac{1}{T^2} e^{-\frac{1}{T}} dT \tag{19}$$

where $P(F)$ is the probability of failure and $P(F|S_T)$ is the conditional probability of failure during the storm of return period T. It is assumed that between storms the piles recover their initial capacity.

The conditional failure probability $P(F|S_T)$, was expressed as a function of storm return period using a relationship of the form

$$-\ln(-\ln(P[F \mid S_T])) = a_0 + a_1 \ln(T) + a_2 (\ln(T))^2 \tag{20}$$

The parameters a_0, a_1 and a_2 were derived in each case from a curve fit of the conditional probabilities obtained from the analyses for the 100 and 1000 year storms. The expression of the conditional probability as a function of return period given by Equation (20) were then substituted into Equation (19) and the required integration performed numerically.

The conditional probabilities of system and component failure for the case where no degradation takes place have been calculated for storms of seven different return periods. This involved little analysis since only the loading model changes with storm return period and not the strength model.

For the degraded cases only two data points are available, corresponding to the 100 and 1000 year return period storms. A quadratic fit was made by noting that, for low return periods, the curves are asymptotic to the zero degradation curve. The curve fits for the three failure criteria are shown in Figure 39, Figure 40, and Figure 41.

An examination of the integrand of Equation (19) showed that the most significant contribution was for values of return period between 10 and 5000 years. Thus the range over which the curve fit was carried out seems appropriate for calculating the total failure probability. However the accuracy of these estimates would be greater if more storms had been analysed.

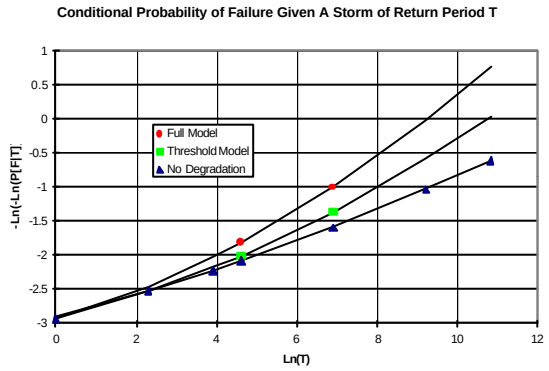

Figure 39 Conditional probability of system collapse, *P(F|T)* for storms of different return period, *T*

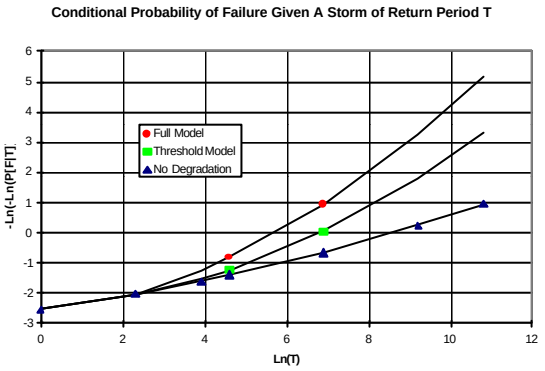

Figure 40 Conditional probability of component failure, *P(F|T)* for storms of different return period, *T*

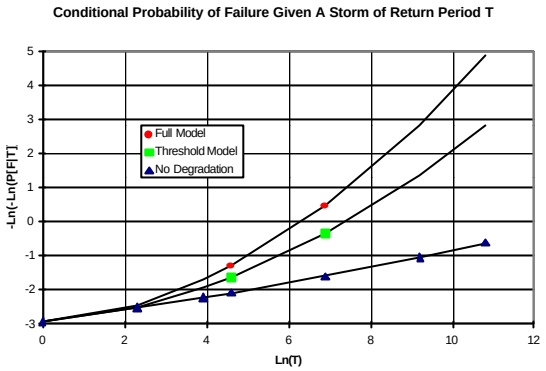

Figure 41 Conditional probability of system failure *P(F|T)* assuming foundation system degradation equals maximum pile degradation for storms of different return period, *T*

The total annual reliability against component failure and overall collapse for the two degradation models are given in Table 16.

Table 16 Annual pile system collapse probability for threshold model

	Component Failure		**System Failure**		**System Failure assuming uniform maximum pile degradation**	
	Annual Reliability Index	**Annual Failure Probability**	**Annual Reliability Index**	**Annual Failure Probability**	**Annual Reliability Index**	**Annual Failure Probability**
No Degradation	**3.1**	**9.3×10^{-4}**	**3.9**	**4.7×10^{-5}**	**3.9**	**4.7×10^{-5}**
Full Degradation Analysis	**2.6**	**4.2×10^{-3}**	**3.4**	**3.1×10^{-4}**	**2.9**	**2.1×10^{-3}**
Analysis with Threshold	**2.9**	**1.9×10^{-3}**	**3.7**	**1.1×10^{-4}**	**3.1**	**9.2×10^{-4}**

The results show that the full degradation model gives failure probability estimates approximately twice those obtained using the threshold model. Since the threshold model is considered to be the currently available best estimate of the degradation process, it will be used for assessing the relative effects of degradation on annual failure probability. A full discussion of the implications of these results is given in Section 11 below.

The annual reliability index against collapse for no degradation is 3.9 corresponding to an annual probability of failure of 4.7×10^{-5}. The annual reliability index against collapse

accounting for degradation using the threshold model is 3.7, giving a failure probability of just over twice that for the undegraded structure of 1.1×10^{-4}. The annual reliability index against component failure is 3.1 corresponding to an annual probability of 9.3×10^{-4}.

The annual reliability estimated assuming that all piles have the same amount of degradation as the most degraded pile reduces from 3.9 to 3.1 when the threshold model is used. This corresponds to an increase in annual failure probability from 4.7×10^{-5} to 9.2×10^{-4}, a twenty-fold increase in failure probability.

11. SUMMARY AND CONCLUSIONS

11.1 Analysis procedure

This study considered the effects of cyclic degradation in the axial capacity of cylindrical driven piles in sand.

A local model for the degradation of shaft frictional shear resistance was implemented into a discretised t-z model of a single pile subject to cyclic axial loading. The local model, originally based on the results of cyclic simple shear tests on sand from a North Sea site, was modified on the basis of a comparison between single pile analysis and full-scale cyclic pile test results. This calibration did not account for the ageing to which the piles in the experiment had been subjected.

The degradation model has the following limitations

- The soil comprises a single layer of sand.
- There is no explicit model for ageing.
- Only regular constant-amplitude cyclic loading is considered.
- Degradation in tip capacity and lateral capacity has not been considered.

Following the initial single pile calibration, the response of an example central North Sea platform was considered. The structural form, foundation layout and loading of the platform were taken from a real structure, but an artificial soil profile was used. The synthetic soil profile was derived to ensure that the design criteria under extreme wave loading for the most stressed pile were just met. The loss in platform capacity during storms of return period 100 years and 1000 years was considered. These storms were discretised into blocks of constant-amplitude waves.

A full degradation analysis of the platform was performed for both storms in which the degradation model was applied regardless of the wave amplitude. The analysis was carried out for storms of 100 and 1000 year return period.

The field work at the Dunkirk site revealed new information regarding the interaction between the ageing and degradation processes which was not known when the analytical work was started. In particular it was seen that low levels of pile cyclic loading can enhance the ageing process and lead to a gain in strength. To account for this, an approximate treatment was applied in which the interaction between degradation and ageing was accounted for using a threshold level of pile cyclic loading below which no cyclic degradation was assumed to occur. The threshold was calibrated against the field test results. Analyses using the degradation threshold were performed for the 100 and 1000 year return period storms.

The structural analysis made the following assumptions

- The effects of long term ageing were ignored.
- The effects of cyclically enhanced ageing were modelled using a threshold on cyclic load amplitude
- The jacket structure remains elastic and, consequently, the interaction between pile and structural failure was not considered.
- The storms were modelled as discrete blocks of constant amplitude waves.
- Waves approached the platform from the broadside direction only.
- The effects of previous storms were ignored.

These limiting assumptions were, for the main part, dictated by the nature of the degradation model. It is considered that the results here obtained represent a reasonable estimate of the amount of degradation to be expected during the analysed storms in the light of the field studies.

11.2 Analysis results

The model with the cyclic loading threshold is considered to be a better model than that which calculates degradation for all wave amplitudes, and the following results and discussion refer to this analysis. Degradation in the capacity of the foundation system was calculated in terms of the following quantities:

1. The degradation in individual pile capacity half way through the storm.
2. The load factor required to cause failure of the first pile, defined in terms of the factor on the extreme 100 year design environmental loading calculated half way through the storm.
3. The Reserve Strength Ratio defined in terms of the factor on the extreme 100 year design environmental loading required to cause collapse of the complete foundation system calculated half way through the storm.
4. Annual probability of failure of a single pile.
5. Annual probability of failure of the foundation system.
6. Annual probability of system failure assuming that the percentage degradation of the overall foundation system capacity equals that of the most severely degraded pile.

The deterministic capacity measures 1, 2 and 3 above are given in Table 17. The reliability-based quantities, 4, 5 and 6 above are given in Table 18 where they are compared with the reliability of the undegraded foundation system.

Table 17 Summary of deterministic results

	1	2	3
	Maximum Reduction in Outer Skirt Pile Capacity	**Reduction in First Pile Failure Load**	**Reduction in RSR**
100 Year Storm	**15%**	**8%**	**5%**
1000 Year Storm	**25%**	**21%**	**14%**

Table 18 Annual probability of pile system collapse

	4		5		6	
	Component Failure		**System Failure**		**System Failure assuming pile system degradation equals that of the most degraded pile**	
	Annual Reliability Index	**Annual Failure Probability**	**Annual Reliability Index**	**Annual Failure Probability**	**Annual Reliability Index**	**Annual Failure Probability**
No Degradation	**3.1**	**9.3×10^{-4}**	**3.9**	**4.7×10^{-5}**	**3.9**	**4.7×10^{-5}**
With Degradation	**2.9**	**1.9×10^{-3}**	**3.7**	**1.1×10^{-4}**	**3.1**	**9.2×10^{-4}**

11.3 Conclusions specific to the platform considered

Taking into account that, for recently driven piles, the threshold treatment represents the current best estimate for cyclic degradation of pile shaft capacity in sands, the following conclusions specific to this analysis may be made.

A. The high degree of redundancy of the pile system led to a considerable increase in capacity above that assumed in design, which is based on a component approach. For the undegraded foundation system, the component failure load factor was 1.9 and the system RSR was 2.95. Specifically, system collapse required mobilisation of the majority of the piles in the system plus mobilisation of the pile head bending resistance before the foundation system failed by overturning. Furthermore, it was found that the design-critical compressive skirt piles attracted little load compared to the other piles once their shaft capacity had been exhausted. This behaviour, which arose from the high redundancy of the foundation system, meant that the analysed

platform had considerable reserves of strength above the levels for which it was designed.

B. The greatest degradation was seen to occur in the tensile capacity of the outer-most skirt piles. This was 15% for the 100 year storm and 25% for the 1000 year storm.

C. The reduction in environmental load factor at first pile failure was 8% for the 100 year storm and 21% for the 1000 year storm. The load factor at first pile failure was influenced by structure-specific system effects, and its value showed a smaller decrease than the individual pile capacity. In particular the presence of constant vertical loading and the redistribution of forces away from the outer-most compressive skirt pile following full mobilisation of its shaft capacity contributed towards making the degradation in the load factor at first component failure lower than the degradation in individual pile capacity.

D. The reduction in system-collapse-based RSR from the threshold analysis was 5% for the 100 year storm and 14% for the 1000 year storm. The reduction in RSR was calculated half way through the storm.

E. A considerable difference between the degradation in individual pile capacity and the degradation in the system-based RSR measure was observed. This difference was primarily governed by the redundancy of the foundation system.

F. The estimated annual probability of both system and component failure of the degraded structure was twice that of the undegraded structure. The effect of degradation was a reasonably small effect in terms of overall probability of failure. However this is a structure-specific measure and is dependent on the overall system redundancy and the extent to which environmental load governs the design.

G. Assuming that the degradation of the complete pile system equals that of the most degraded pile, the annual reliability index was estimated to reduce from 3.9 for the undegraded foundation system to 3.1 for the degraded foundation system, corresponding to a twenty-fold increase in annual failure probability from 4.7×10^{-5} to 9.2×10^{-4}. This relative increase would be expected for platforms with minimal redundancy in the foundation system and for which the pile design is governed by the overturning effects arising from the extreme environmental load case. For such structures, overall collapse is governed by the first pull-out or tensile pile failure.

11.4 Generic Conclusions

These conclusions are based on the results of the analysis with the degradation threshold and relate to sands with no long-term ageing.

As has been seen, the platform considered in this study was not critical with respect to the effects of degradation on its overall foundation capacity. The system RSR was seen to be reduced by 5% as a consequence of degradation in the 100 year return period storm. The maximum degradation in a single pile was 15% for the tensile capacity of the outer-most

skirt pile. For platforms with few piles for which system failure is governed by the first pile failure, this figure of 15% can be assumed to be an appropriate measure of the degradation in total structural capacity. This would correspond to a twenty-fold increase in annual failure probability arising from degradation. This is a quite significant increase in failure probability, and could very well have implications for the integrity of platforms with non-redundant foundation systems.

On the basis of this study, a number of factors have been identified as having a possible impact on the overall effects of wave-induced pile capacity degradation. These are listed in the following:

A. **Foundation system redundancy.** This is the major contributor to the difference between individual pile degradation and foundation system degradation observed in this analysis. Reduction of the pile system redundancy could result in the proportional degradation of the complete pile system which is the same as that for an individual pile.

B. **Increased criticality of environmental load in pile design**. For some platforms, the relative proportion between dead and environmental loading may be higher than for the example platform analysed here. This will result in a foundation system in which the pile is designed to resist a higher proportion of wave loading to dead loading than in this example. Waves passing through the platform will lead to cyclic loading which is a higher proportion of the pile capacity than in this example. This will lead to a greater amount of degradation as a proportion of capacity than for the example platform.

C. **Decrease in shaft capacity relative to tip capacity.** This will lead to complete load reversals over the whole pile length at a lower level of cyclic loading than for the example platform. This may lead to a relative increase in shaft degradation. The effect could, however, be offset by the increase in tip capacity which does not degrade.

D. **Design-criticality of piles in tension.** Increased design criticality of tension piles, for which shaft friction degrades over the whole length, could lead to greater cyclic loading down the pile and thus greater individual degradation.

12. RECOMMENDATIONS FOR FUTURE WORK

This pilot study has highlighted a number of areas which indicate significant effects of short-term degradation on a foundation system. Although the system considered was by no means critical as regards its sensitivity to degradation induced by cyclic loading, a number of important features were highlighted.

12.1 Soil modelling

During the course of the study, and as more experimental results were obtained, it became clear that there is considerable complexity in the interaction between long-term ageing of piles and their response to cyclic loading events. These effects require considerably more study for them to become fully understood.

The soil model considered in this study was developed for blocks of constant amplitude cyclic loading. In a realistic storm scenario, a platform is subject to a variable amplitude loading which could lead to a different degradation ratio. This effect should be further studied.

The present model is applicable only to sand. The effects of cyclic loading on clays and layers of mixed sands and clays should also be considered.

12.2 Storm modelling and reliability

The capacity of the foundation system has been found to depend on a complex interaction between ageing and degradation. Storm events can give rise to degradation or enhanced ageing, with ageing also occurring between storms. The full nature of this behaviour is not yet fully understood, and work should be directed first towards a deeper understanding of these phenomena, and then towards how this understanding can be combined with the random environmental models. This will then provide a means of calculating the foundation system failure rate expressed in terms of the probability of foundation system failure.

The following aspects are important for the derivation of the annual failure probability given appropriate models for pile capacity ageing and degradation interaction:

1. **Storm history**. The random storm history will influence the capacity of the foundation system given that prior storms will give rise to an interaction between degradation and ageing and that ageing will occur between storms.

2. **Age of the platform**. The annual failure probability (failure rate) is a function of the age of the platform, given that the foundation capacity is dependent on storm history and time. An assessment of annual failure probability at different times in the platform lifetime is required. This will entail the investigation of the probabilities of collapse given alternative scenarios of prior storms and collapse storms, and the derivation of the probability of occurrence of these scenarios.

12.3 Structural analysis

There is a wide variety of loading conditions, structural types, foundation systems and soil types present in the North Sea, each combination of which may show a different sensitivity to degradation effects. It was seen that the structural system considered in this study was by no means critical. It possessed a high degree of redundancy in the foundation system which led to a considerably higher value in the undegraded foundation capacity over and above the design criteria. It was found that, because of this redundancy, only the outermost piles significantly lost capacity. The result was a small loss in overall pile system capacity.

For other foundation systems this loss could be much more prominent and thus and improved understanding of the degradation of a variety of different foundation systems is urgently needed. It is important to study a wider variety of structural types and soil profiles. In particular the following aspects are important:

1. **Redundancy of the pile system**. Many platforms have very little pile system redundancy. This makes foundation failure more design-critical and also results in a larger effect of the overall degradation.

2. **Criticality of the environmental loading on pile design.** The relative proportions of dead and environmental load influence the ratio between cyclic load amplitude and pile capacity. This will influence the amount of pile degradation.

3. **Soil profile**. The effects of different soil layering is important in influencing the spread of the high amplitude cyclic load reversals down the pile.

4. **Pile geometry.** The effect of pile geometry influences the relative stiffness between pile and soil and the consequently the spread of skin friction capacity mobilisation down the pile. Piles with low D/t ratios will be relatively stiffer and will experience full cyclic reversal over a greater proportion of their length.

5. **Lateral soil behaviour.** The effect of variations in the lateral soil stiffness and capacity may affect the cyclic axial loading down the pile, and the degree of degradation. Furthermore, the discrete spring models do not take account of any local interaction between axial and lateral pile capacity, stiffness, degradation and ageing.

13. REFERENCES

[1] Jardine, R.J. and Standing, J.R, "Final report on HSE funded cyclic loading study", for Imperial College Consultants (ICON), March 1999.

[2] Jardine, R.J., "Interim Report on Cyclic Loading Model and Synthetic Soil Profile for HSE Funded Pile Cyclic Loading Study", for Imperial College Consultants (ICON), October 1998.

[3] Jardine, R.J. and Standing J.R., "Report on pile testing performed for HSE cyclic loading study and EU funded GOPAL project at Dunkirk, France,. Phase 3, April-May 1999", for Imperial College Consultants (ICON).

[4] Jardine R.J. and Chow F.C., "New Design Methods for Offshore Piles", Marine Technology Directorate, 1996.

[5] "Mathcad 8 User's Guide", Mathsoft 1998.

[6] "API Recommended practice for Planning, Designing and Constructing Fixed Offshore Platforms-Working Stress Design", 20th Edition, *American Petroleum Institute*, 1993.

[7] ISO TC 67/SC7/WG3 Annex 1."Metocean Criteria" Draft.

Printed and published by the Health and Safety Executive
C0.5 12/00

MAIL ORDER
HSE priced and free
publications are
available from:
HSE Books
PO Box 1999
Sudbury
Suffolk CO10 2WA
Tel: 01787 881165
Fax: 01787 313995
Website: www.hsebooks.co.uk

RETAIL
HSE priced publications
are available from
good booksellers

HEALTH AND SAFETY INFORMATION
HSE InfoLine
Tel: 08701 545500
or write to:
HSE Information Centre
Broad Lane
Sheffield S3 7HQ
Website: www.hse.gov.uk

OTO 2000/013

£25.00

ISBN 0-7176-1911-7